VILNIUS UNIVERSITY
CENTER FOR PHYSICAL SCIENCES AND TECHNOLOGY

RIMVYDAS VENCKEVIČIUS

COMPACT SPECTROSCOPIC TERAHERTZ IMAGING SOLUTIONS USING GaAs/AlGaAs AND InGaAs SEMICONDUCTOR NANOSTRUCTURES

Summary of doctoral dissertation
Physical Sciences, Physics (02 P)

Vilnius, 2016

Dissertation was prepared in 2011 - 2016 at the Semiconductor Physics Institute of Center for Physical Sciences and Technology.

Scientific supervisor:

prof. habil. dr. Gintaras Valušis (Center for Physical Sciences and Technology, Physical Sciences, Physics - 02 P).

Scientific advisor:

dr. Irmantas Kašalynas (Center for Physical Sciences and Technology, Physical Sciences, Physics - 02 P).

Doctoral thesis will be defended in the joint council of Vilnius University and Center for Physical Sciences and Technology of physical sciences:

Chairman:

prof. habil. dr. Saulius Juršėnas (Vilnius University, Physical Sciences, Physics - 02 P).

Members:

prof. habil. dr. Žilvinas Kancleris (Center for Physical Sciences and Technology, Physical Sciences, Physics - 02 P);

prof. habil. dr. Jerzy Łusakowski (University of Warsaw, Physical Sciences, Physics - 02 P);

prof. habil. dr. Gintautas Tamulaitis (Vilnius University, Physical Sciences, Physics - 02 P);

prof. habil. dr. Sigitas Tamulevičius (Kaunas University of Technology, Physical Sciences, Physics - 02 P).

The dissertation will be defended under open consideration in the council of physics at 14 h on 20th June, 2016, at the Center for Physical Science and Technology, Address: room D401, Saulėtekio ave. 3, LT-10222 Vilnius, Lithuania

Summary of doctoral dissertation has been distributed on May 20, 2016.

The dissertation is available in Vilnius University, Center for Physical Science and Technology libraries and in VU web site: www.vu.lt/lt/naujienos/ivykiu-kalendorius

VILNIAUS UNIVERSITETAS
FIZINIŲ IR TECHNOLOGIJOS MOKSLŲ CENTRAS

RIMVYDAS VENCKEVIČIUS

KOMPAKTIŠKO SPEKTROSKOPINIO TERAHERCINIO VAIZDINIMO SPRENDIMAI, NAUDOJANT GaAs/AlGaAs IR InGaAs PUSLAIDININKINIUS NANODARINIUS

Daktaro disertacijos santrauka
Fiziniai mokslai, fizika (02 P)

Vilnius, 2016

Disertacija rengta 2011 - 2016 metais Fizinių ir technologijos mokslų centro Puslaidininkių fizikos institute.

Mokslinis vadovas:
prof. habil. dr. Gintaras Valušis (Fizinių ir technologijos mokslų centras, fiziniai mokslai, fizika - 02 P).

Mokslinis konsultantas:
dr. Irmantas Kašalynas (Fizinių ir technologijos mokslų centras, fiziniai mokslai, fizika - 02 P).

Disertacija ginama jungtinėje Vilniaus universiteto ir Fizinių ir technologijos mokslų centro fizinių mokslų krypties taryboje:

Pirmininkas:
prof. habil. dr. Saulius Antanas Juršėnas (Vilniaus universitetas, fiziniai mokslai, fizika - 02 P).

Nariai:
prof. habil. dr. Žilvinas Kancleris (Fizinių ir technologijos mokslų centras, fiziniai mokslai, fizika - 02 P);
prof. habil. dr. Jerzy Łusakowski (Varšuvos universitetas, fiziniai mokslai, fizika - 02 P);
prof. habil. dr. Gintautas Tamulaitis (Vilniaus universitetas, fiziniai mokslai, fizika - 02 P);
prof. habil. dr. Sigitas Tamulevičius (Kauno technologijos universitetas, fiziniai mokslai, fizika - 02 P).

Disertacija bus ginama viešame Fizikos mokslų krypties tarybos posėdyje 2016 m. birželio 20 d. 14:00 val. Fizinių ir technologijos mokslų centre, D401 kab. Saulėtekio al. 3, LT-10222 Vilnius, Lietuva.

Disertacijos santrauka išsiuntinėta 2016 m. gegužės mėn. 20 d.
Disertaciją galima peržiūrėti Vilniaus universiteto, Fizinių ir technologijos mokslų centro bibliotekose ir VU interneto svetainėje adresu: www.vu.lt/lt/naujienos/ivykiu-kalendorius.

Acknowledgment

First of all I am very grateful to my supervisor Gintaras Valušis, who has not only helped me throughout my research in PhD studies, but also gave me a very good start in scientific career by inviting me to participate in thematics of Terahertz physics.

I am also very grateful to my scientific adviser Irmantas Kašalynas for invaluable consultations in spectroscopic terahertz imaging and Fourier spectroscopy experiments and to Liudvikas Subačius for the help in microwave and nanosecond pulse experiments. I would also like to thank Linas Minkevičius for the preparation of sample contacts, and also to all Teraherz Photonics laboratory group in Center for Physical Science and Technology for kind cooperation in generation and implementation of new scientific ideas.

I appreciate Kirill Alekseev for his theoretical input analyzing experimental results.

I am grateful to Alvydas Lisauskas and all other members of prof. Hartmur Roskos group for welcoming me to a very valuable summer internship in Physics institute of J.W. Goethe university (Frankfurt/M, Germany) in Frankfurt.

I would like to thank my wife Judita and my mother Elytė for endless total support through all years of studies.

Introduction

Terahertz (THz) radiation corresponds to electromagnetic spectrum lying between microwaves and infrared at frequency range from 0.1 to 30 THz ($1\,\mathrm{THz} = 10^{12}\,\mathrm{Hz} \equiv 4\,\mathrm{meV}$). Most organic materials, chemical compositions, biological agents exhibit spectral fingerprints in this region. However, THz range is rather complicated to implement into practice because operation principles for devices are neither truly electronic, nor truly optical. Progress in development of coherent THz Time-Domain (TDS) spectroscopy systems in last decade allowed to exploit this frequency range in various scientific as well as numerous practical applications [1]. Although coherent systems exhibits very large dynamic range, they are not very well suited for fast and compact THz imaging systems due to necessity to measure THz impulse waveform. That is why non-coherent THz imaging systems with fast operation are considered for practical applications (such as security systems, quality control, etc.). Possible option would be to avoid coherent detection, but this would require new more powerful emitters and amplifiers and/or more sensitive detectors. Therefore, beam shape of THz emitter and its influence on image quality is also rather relevant, especially when dimensions of emitter is decreased below wavelength and additional beam shaping may add some power loss.

As for modern room temperature THz emitters, Quantum Cascade Lasers (QCL) with intracavity difference-frequency generation are now of particular interest [2]. However, these devices operate at higher frequencies ($\approx 3\,\mathrm{THz}$), but for practical needs, longer penetration depth is needed, hence, frequencies below 1 THz are of preference. Invention of Molecular Beam Epitaxy technology stimulated huge scientific interest in artificial materials, having desirable properties defined rather by materials layer thickness than properties itself. One of the exciting options in materials engineering was semiconductor superlattices (SL) as a medium to excite Bloch oscillations (BO) as it was suggested by Esaki-Tsu in 1971 [3].They were discovered in optical experiments, however, still neither scientific works revealing signatures of electrically pumped BO nor Bloch lasing are published.

Special technological requirements are considered for spectroscopic THz imaging systems essential for practical applications allowing one direct determination of material composition without measuring full spectrum. For real-time operation fast response broadband THz detectors or cameras with a few color pixels are required. Recent development of THz detectors resulted with some high performance sensors, such as Schottky diodes and field effect transistors, but complicated technology determines high prices of such devices. THz sensors displaying good sensitivity, fast

operation speed, resistant to electrostatic noise, suitable for array fabrication, and manufactured by industrial low cost technology remains an important issue. Also, the preference would be devoted to planar technology solutions.

This doctoral thesis concentrates on finding, investigating, and applying new solutions for fast, compact, relatively easy to use, room-temperature spectroscopic imaging systems. Comprehensive complex study was carried out involving all main devices of THz imaging systems including sources, amplifiers, optical components and detectors. Main results of this work are distributed throughout 4 main chapters.

In the 1st chapter the results of experimental study on THz surface emitter based on *p-i-n-i*-type AlGaAs/GaAs heterostructure designed by A. Reklaitis [4] are presented. The 2nd chapter is dedicated to consistent investigation of AlGaAs/GaAs superlattice diode as a medium with strong homogeneous electric field required for the manifestation of stable and modulated Bloch gain. In the 3rd chapter experimental study revealing how usage of multimode laser source influences quality of THz images. Spectroscopic THz imaging system employing TEM_{01} laser mode was applied for the THz imaging of silicon solar cells. The last 4th chapter of the thesis is dedicated to the investigation and application of new innovative non-coherent THz detector solutions. Using spectroscopic imaging the principal component analysis of explosive simulators based on sucrose and tartaric acid was carried out. In such experiment broadband bow-tie InGaAs diodes and resonant antenna-coupled field effect transistors were used as THz sensors for the first time. As for THz imaging systems with optoelectronic emitters, usually used in coherent THz time-domain systems, non-coherent sensitive low noise sensors based on titanium microbolometers were applied for spectroscopic imaging of samples made of lactic acid and tartaric acid compounds.

Main goal and objectives

Main goal of this doctoral thesis is to find, investigate, and apply new solutions for compact room temperature spectroscopic imaging systems for terahertz frequency range based on solid state components.

To achieve this goal the following **objectives** were addressed:

1. Experimental investigation of terahertz surface emitter based on delta-doped *p-i-n-i* GaAs/AlGaAs heterostructure exciting it with femtosecond optical pulses and compare its operational characteristics with InGaAs and InAs surface emitters.

2. Development of electrically pumped environment suitable for the manifestation and experimental observation of Bloch gain:
    a) adaptation of controlled injection theoretical principles, similar to sub-critical Gunn amplifiers, to the superlattice-based diode.
    b) theoretical determination of conditions necessary to form homogeneous electric field profile in semiconductor superlattice;
    c) application of nanosecond DC voltage pulses together with microwave techniques for the investigation of high electric field induced phenomena in semiconductor superlattice, development of fast computer controlled data acquisition software required to realize experiment;
    d) investigation of high electric field induced Bloch gain signatures in microwave frequency range in semiconductor GaAs/AlGaAs superlattices.
3. Investigation of spatial resolution and applicability of imaging systems using terahertz radiation source with higher order beam mode.
4. Exploration of innovative compact teraherz radiation detector solutions and their applicability for spectroscopic imaging in a direct detection mode.

Scientific novelty

Scientific novelty of this work is based on the following statements.

1. For the first time delta-doped *p-i-n-i* GaAs/AlGaAs heterostructure designed for efficient emission of terahertz radiation under excitation with femtosecond optical pulses by A. Reklaitis (Phys. Rev. B 77, 153309, 2008) was experimentally investigated. It was revealed that such structures are effective terahertz emitters which efficiency under certain conditions is better than InGaAs and InAs surface emitters.
2. Diodes based on strongly coupled Silicon doped GaAs/AlGaAs superlattices with injection limited contacts designed to create environment suitable for Bloch gain manifestation were investigated both theoretically and experimentally:
    a) using similar theoretical principles as for injection controlled sub-critical Gunn amplifiers, the analytical model was proposed for superlattice diode, allowing to find suitable condition to implement homogeneous electric field profile necessary for Bloch gain;
    b) it was experimentally shown that using injection controlled GaAs/AlGaAs superlattice diode stable and modulated Bloch gain can be observed in microwave frequency range at room temperature.

3. TEM_{01} laser mode was applied for THz imaging of silicon solar cells. It was shown that for given multi-mode laser operation the proper selection of focusing optics allows one to write high quality images.
4. Innovative compact THz radiation detectors were applied in direct detection spectroscopic imaging:

    a) asymmetrically-shaped InGaAs diodes were applied for spectroscopic imaging in the frequency range of 0.5–2.52 THz and employing principal component analysis explosive simulators fabricated from sucrose and tartaric acid were identified;
    b) frequency range for spectroscopic THz imaging was extended up to 4.25 THz using patch-type antenna-coupled field effect transistors as THz sensors exploiting plasmonic mixing phenomenon;
    c) non-coherent room temperature detectors based on titanium microbolometers were applied in spectroscopic imaging system with optoelectronic THz emitter.

Statements to defend

1. Delta-doped *p-i-n-i* GaAs/AlGaAs heterostructures excited by femtosecond laser pulses are effective terahertz radiation emitters with emitted power exceeding power emitted by InGaAs and InAs surface emitters if optical pump fluence does not exceed $0.7\,\mu J/cm^2$ and $7\,\mu J/cm^2$ for pump pulse repetition rate of 82 MHz ir 1 kHz, respectively.
2. Asymmetric injecting/blocking contacts – Schottky contact and heterostructure - can be used to create homogeneous electric field in GaAs/AlGaAs superlattice within a range of applied bias voltage values. Under these conditions in strongly coupled GaAs/AlGaAs superlattice diode Bloch gain can be observed.
3. The use of focusing optics with short focal distance in the imaging system with a radiation source emitting TEM_{01} beam mode of terahertz radiation allows one to record good quality terahertz images with spatial resolution close to the diffraction limit.
4. InGaAs bow-tie diodes are suitable for room temperature active spectroscopic imaging in terahertz frequency range under the conditions of emitters operating in milliwatts power range. Upper limit of imaging frequency range is determined by electron momentum relaxation time. Frequency range for spectroscopic imaging can be extended using plasmonic mixing in nanometer field effect tran-

sistors.

5. Non-coherent room temperature detectors are suitable for spectroscopic imaging systems with optoelectronic terahertz radiation emitters if their noise equivalent power is in order of 10 pW/$\sqrt{}$Hz.

1 Coherent terahertz radiation emission from photoexcited electron-hole plasma

Wide bandwidth terahertz radiation emitted from photoexcited semiconductor surfaces with femtosecond laser pulses [5] is widely used for spectroscopic needs. Under high-repetition-rate excitation conditions the best THz surface emitter is known to be *p*-type InAs due to a combination of strong optical rectification and a pronounced photo-Dember effect. Other materials like *n*-type InAs and InGaAs was found to be of lower efficiency [6]. If one considers emitters employing transient photocurrents in surface depletion fields , such as *p-i-n* GaAs or low temperature grown GaAs, its efficiency is limited because only a part of excited carriers contributes to the transient current. Reasons for this are (I) the exited region extends far beyond the surface-field region, and (II) the built-in electric field may rapidly be screened by the excited photocarriers. Second, the plasma frequency of the excited carriers depends on photoexcited carrier density as $\omega = \sqrt{\omega_P^2 - \gamma^2/4}$, where $\omega_P = \sqrt{\frac{e^2 n}{\varepsilon_0 m^*}}$ frequency of undamped plasma and γ is momentum relaxation rate. Due to that plasma frequency is position-dependent both in vertical and horizontal directions. Therefore, the amplitude of the resulting transient current rapidly drops due to interference effects [4]. To improve the efficiency of emitters, the electric-field and absorption profiles need to be optimized. A new type of efficient THz emitter, based on cascade *p-i-n-i* GaAs/AlGaAs heterostructure, was suggested by A. Reklaitis [4].

In this work experimental investigation of such emitter was carried out. Optimal excitation conditions were found and emission from *p-i-n-i* heterostructure was compared with that of *p*- and *n*-type InAs and InGaAs emitters.

1.1 GaAs/AlGaAs *p-i-n-i* emitter

For the experiment GaAs/AlGaAs *p-i-n-i* heterostructure was grown by K. Köhler[1] using molecular beam epitaxy. Heterostructure design was calculated by A. Reklaitis[2].

[1] Fraunhofer-Institut für Angewandte Festköperphysik, Freinburg, Germany
[2] Center for Physical Science and Technology, Lithuania

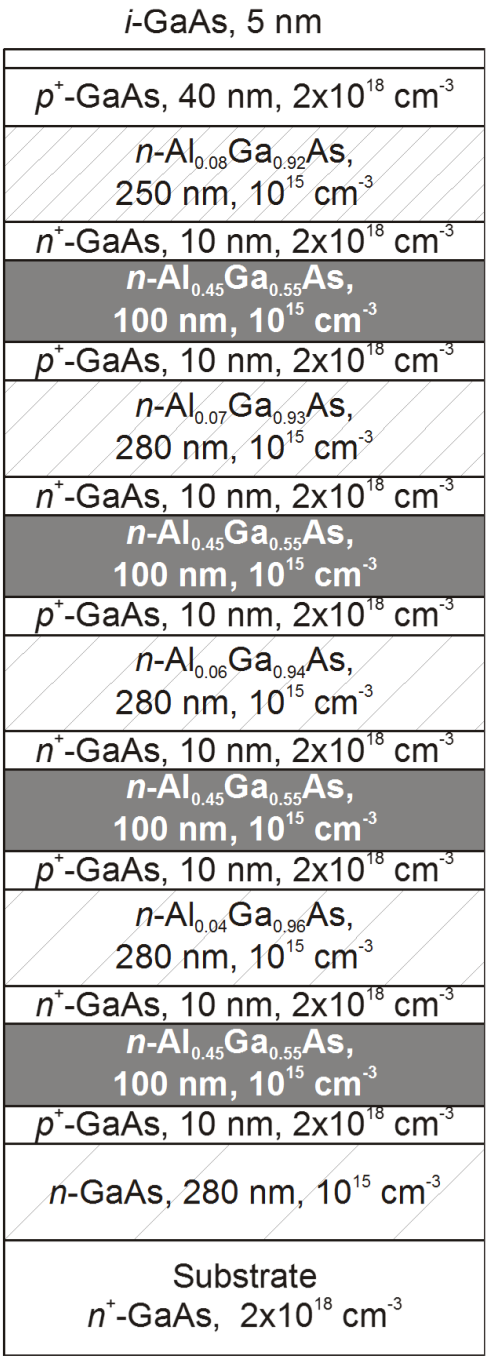

Figure 1. Design of $Al_xGa_{x-1}As$/ $Al_{0.45}Ga_{0.55}As$ heterotructure terahertz emitter.

A plot with the design of heterostructure is shown in Fig. 1. It is composed of five periods of unintentionally doped $Al_xGa_{x-1}As/Al_{0.45}Ga_{0.55}As$ layers. Alternating n- and p-type δ-doped GaAs layers are inserted at the $Al_xGa_{x-1}As/Al_{0.45}Ga_{0.55}As$ interfaces. The different aluminium mole fractions x of the $Al_xGa_{x-1}As$ layers ranging from 0.08 (top, $\varepsilon_g = 1.524\,\mathrm{eV}$) to 0.00 (bottom, $\varepsilon_g = 1.424\,\mathrm{eV}$) are selected to ensure equal average electron and hole densities in each layer after photo-excitation. This is achieved by means of a slight increase of the absorption coefficient α_i in the $Al_xGa_{x-1}As$ layers, thus counteracting the decrease of excitation intensity with inc-

reasing penetration depth. α_i values for each optically-active layer are 0.55; 0.65; 0.75; 0.95 and $1.25\,\mu m^{-1}$, respectively, for wavelength $\lambda = 800\,nm$. Inverse absorption coefficient α_i^{-1} exceeds layer thickness $L = 0.30\,\mu m$, so that the condition $\alpha_i L \ll 1$ is satisfied, meaning homogeneous distribution of photocarriers in each layer.

When heterostructure is excited by optical pulse, carriers are generated only in the $Al_xGa_{x-1}As$ layers, while their movement in z-direction is restricted due to the presence of the $Al_{0.45}Ga_{0.55}As$ barriers. Due to the strong internal electric fields the photo-carriers are accelerated in their separate layers simultaneously which drives a coherent plasma oscillation resulting in an enhanced THz emission.

1.2 Experiment

Experiment setup for THz emission excitation is shown in Fig. 2. Femtosecond Ti:sapphire laser pulses were focused on the surface of emitter. So called z-scan technique was implemented to vary excitation density via changing the distance between the sample and the focusing lens. The emitted radiation was collected by a parabolic mirror. The power of the emitted THz radiation was measured by either a liquid-helium-cooled bolometer or a Golay cell. The setup was purged with N2 gas or dry air in order to avoid absorption by water vapor.

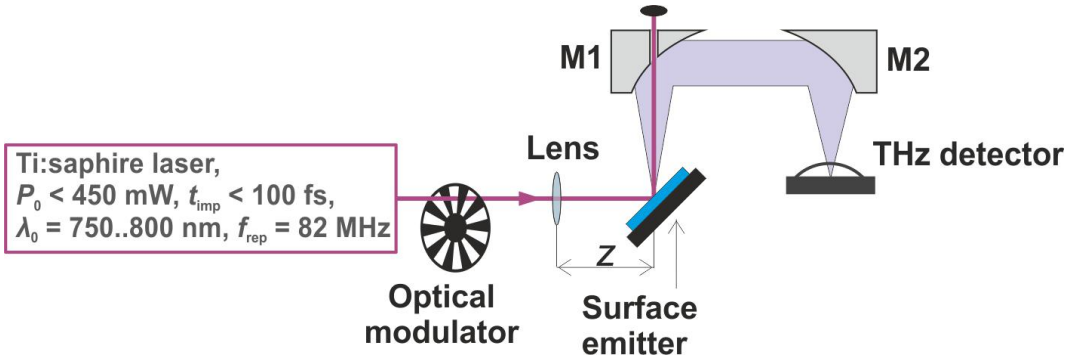

Figure 2. Experiment setup used for the excitation of THz emitters.

Initially the optimal excitation conditions were determined. By changing center of the wavelength and pump power of the high-repetition-rate Ti:sapphire laser ($f_{rep} = 82\,MHz$, $\tau_{pulse} < 100\,fs$), it was established that the highest power of the THz radiation ($1.25\,\mu W$ at the pump power of $400\,mW$) was found around 780 nm. Using this wavelength z-scan experiments were carried out for p-i-n-i heterostructure and compared with (111)-oriented p-type InAs ($N_A = 2 \times 10^{16}\,cm^{-3}$), (100)-oriented n-type InAs ($N_D = 2 \times 10^{16}\,cm^{-3}$) and undoped (100)-oriented $In_{0.53}Ga_{0.47}As$ (thickness $500\,nm$) emitters excited under the same conditions.

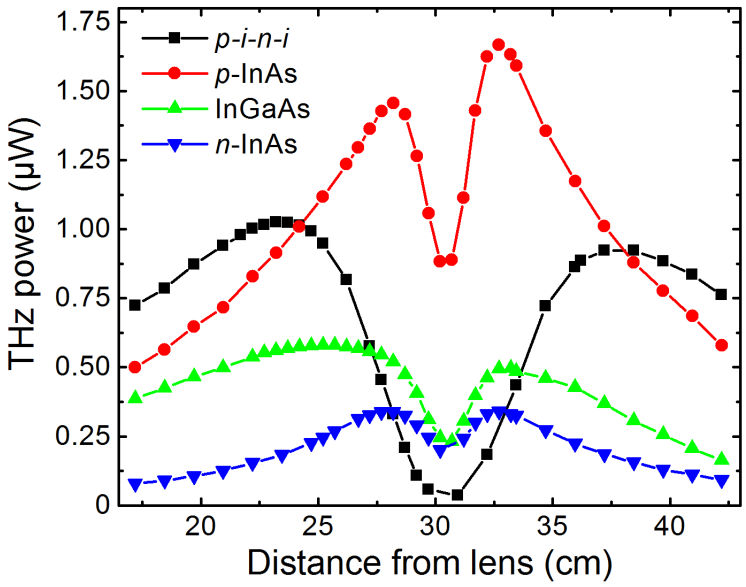

Figure 3. Emitted THz power dependence on the distance between sample and lens measured with z-scan technique. Data for GaAs/AlGaAs *p-i-n-i* heterostructure is compared with InAs and InGaAs emitters. $\lambda_0 = 780\,\text{nm}$, $P_0 = 450\,\text{mW}$, lens focal distance is 30.5 cm. [A5]

Experimental results using z-scan technique is presented in Fig. 3. It is seen that at low optical fluences ($z < 23\,\text{cm}$), the $Al_xGa_{x-1}As/Al_{0.45}Ga_{0.55}As$ emitter is found to deliver the highest THz output power outperforming even the p-InAs emitter. The emission from the $Al_xGa_{x-1}As/Al_{0.45}Ga_{0.55}As$ emitter peaks at an optical fluence of $0.7\,\mu\text{J/cm}^2$, but then it saturates and decreases much earlier than for all other emitters (InGaAs: $1.4\,\mu\text{J/cm}^2$, n-InAs: $5.5\,\mu\text{J/cm}^2$, p-InAs: $8.5\,\mu\text{J/cm}^2$). In all cases, saturation results from the screening of the internal fields.

Screening of the internal fields by photo-exited carriers is one of the main effects limiting maximum emission power of surface THz emitters. As it is seen from z-scan results (Fig. 3) electric field screening leads to a dip in the THz power curve. For the *p-i-n-i* emitter screening effect is much more pronounced than that for other emitters. The reason behind this is long-lived charge carriers, because in the designed heterostructure photo-exited electrons and holes are separated spatially making thus recombination rather complicated.

In order to prove the aforesaid effect additional measurements were carried out using low-repetition-rate laser system [7] (1 kHz instead of 82 MHz) with time-domain electro-optical detection. In this case longer time between pump pulses allows carrier to recombine, thefore, and screening by surviving carriers should drastically reduced. Experimental data for low-repetition-rate excitation case are given in Fig. 4.

In this case $Al_xGa_{x-1}As/Al_{0.45}Ga_{0.55}As$ emitter saturates at 10 times higher optical

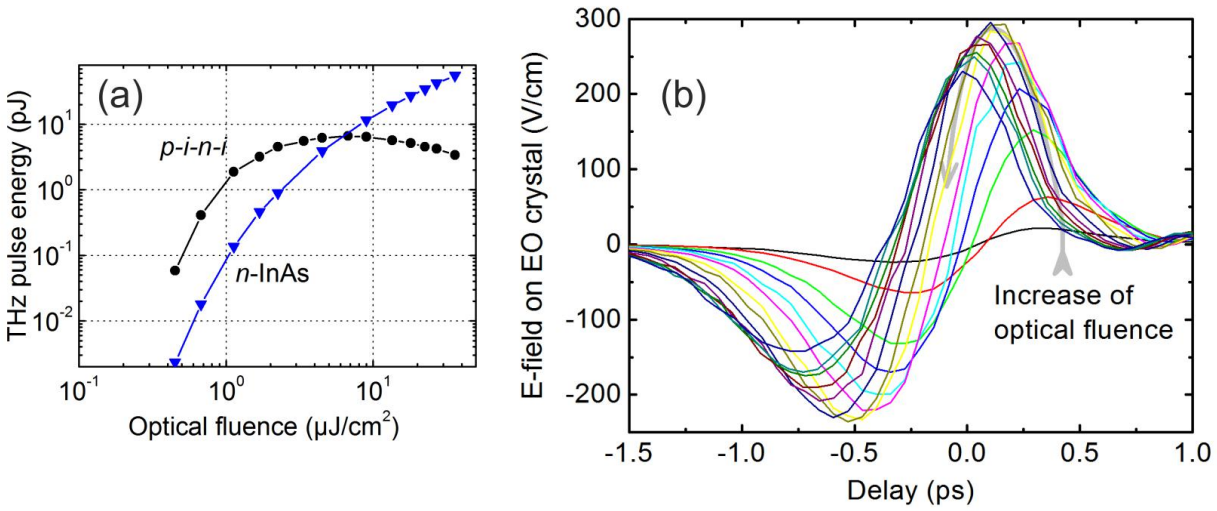

Figure 4. (a) THz pulse energy values and (b) THz waveforms measured with low-repetition-rate excitation from the *p-i-n-i* heterostructure for a series of optical fluences from 0.45 J/cm^2 to nearly 40 J/cm^2. [A5]

fluence of 7 μJ/cm^2 compared with high-repetition-rate case presented earlier. With lower repetition rate screening of electric field is caused by carriers excited during one pump pulse instead of over many pulse cycles. This is proven by the measured THz waveforms shown in Fig. 4b. With rising optical fluence, around the saturation point, the THz pulse is emitted earlier, shifting forward in time by several hundred femtoseconds. This shift reflects the faster field dynamics at higher fluence, with the consequence that the trailing part of the optical pulse contributes less and less to THz emission because the internal field is screened more and more already by the carriers excited by the leading part of the pulse.

The peak field reaches 300 V/cm (corresponding to a pulse energy of 8 pJ) when the radiation is focused. As it is shown in Fig. 4a, the pulse energy remains higher than that of the *n*-InAs sample up to the saturation point.

To summarize, for the first time THz surface emitter based on δ-profile doped *p-i-n-i* $Al_xGa_{x-1}As/Al_{0.45}Ga_{0.55}As$ heterostructure was experimentally demonstrated. Under excitation of femtosecond laser pulses z-scan technique was used to find optimal excitation conditions. Obtained results were compared with InAs and InGaAs emitters measured under same excitation conditions. It was shown that THz emission power from *p-i-n-i* emitter exceeds THz power emitted from InAs and InGaAs emitters if excitation optical fluece does not exceed 0.7 μJ/cm^2 and 7 μJ/cm^2 for pump pulse repetition rate of 82 MHz and 1 kHz, respectively. THz emission power can be increased with increasing carrier recombination rate. Solving this problem may display *p-i-n-i* heterostructure emitter as a promising alternative to InAs THz

emitters.

From the results presented in this chapter *the 1st statement to defend* was formulated: Delta-doped *p-i-n-i* GaAs/AlGaAs heterostructures excited by femtosecond laser pulses are effective terahertz radiation emitters with emitted power exceeding power emitted by InGaAs and InAs surface emitters if optical pump fluence does not exceed $0.7\,\mu J/cm^2$ and $7\,\mu J/cm^2$ for pump pulse repetition rate of $82\,MHz$ and $1\,kHz$, respectively.

2 Signatures of Bloch gain in microwave frequency range in controlled injection superlattice diode

Semiconductor superlattices (SL) are artificial periodic structures consisting of alternating layers with different thickness. Esaki-Tsu suggested to use SL as an environment to explore different physical phenomena of quantum origin in a solid state or employ them as essential ingredient in modern devices including generation and amplification of microwave and terahertz frequencies [3]. SL served as environment to realize Bloch oscillations – quantum beats with spatial displacement excited by femtosecond laser pulse [8]. In a stationary electrical transport approach, the Bloch oscillations reveal themselves in terms of negative differential mobility (NDM) for electric fields larger than some critical value. A device employing these features of superlattice – electrically-pumped Bloch oscillator – is still not realized up to now. On the other hand, from the point of view of modern devices, tailoring of electronic transport in SL were successfully employed in realization of quantum cascade lasers (QCLs) [9].

In contrast to QCLs operating at fixed frequencies, inherent feature of Bloch gain is a broadband operation – the effect allows one to amplify electromagnetic radiation (optical gain) below the Bloch frequency [10]. To realize the Bloch gain very high and at the same time homogeneous as much as possible electric fields are needed. In real experimental situations, the electric field is far from homogeneity [11] or its homogeneity exists within a very short time, e. g. 10 ps scale[12].

The issue of the inhomogeneity of the electric field was known for a long time in other type of semiconductor devices with NDM – in sub-critically doped Gunn diodes [13]. It is worth noting, however, that if the Kroemer criterion, $n \times L$, is less than some critical value, despite of NDM regime, moving electric field domains does not form. In order to set the operation into broadband gain dominated by NDM mechanism, one needs to make electric field more spatially homogeneous and avoid formation of undesirable regions with local fields strengths falling below the critical value. To overcome the problem energy barriers were introduced at the injecting contact into the devices [14]. In more general case, however, both dc and ac currents in the stable amplifier will be determined not only by bulk space charge in the active region, but also by properties of attached contacts [15].

In this chapter of thesis, investigation of injector-controlled strongly-coupled GaAs/AlGaAs superlattice diode designed for experimental observation of Bloch gain was carried out. Design of molecular beam epitaxy grown SL based on $GaAs/Al_{0.3}Ga_{0.7}As$

heterostucture is shown in Fig. 5. SL was designed to have wide miniband of 104 meV, enabling thus stable operation up to electric field strength of $31E_{cr}$, where $E_{cr} = 5.5\,\mathrm{kV/cm}$ is Esaki-Tsu critical field. Length of active layers ($L = 236\,\mathrm{nm}$) and doping density ($N_d = 10^{16}\,\mathrm{cm}^{-3}$) was selected to satisfy stability criterion $\alpha = \frac{en_dL}{\varepsilon_0\varepsilon_r E_{cr}} = 5.7 < 7$ to avoid formation of electric field domains.

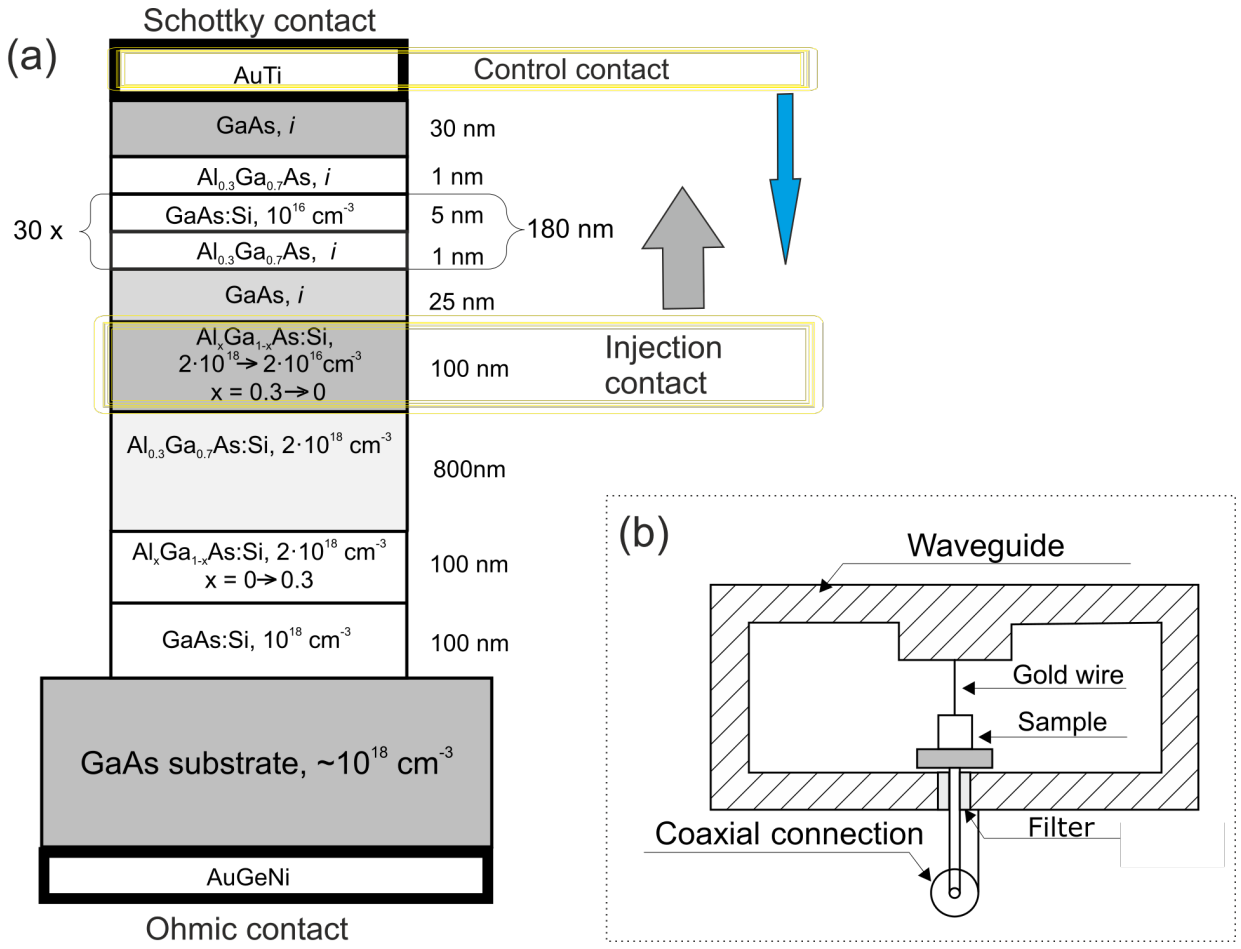

Figure 5. Architecture of GaAs/AlGaAs superlattice diode (a). Cross-section view of sample placement in waveguide (b).

The SL structure is embedded between asymmetrically designed non-ohmic contacts – the Schottky and the heterostructure ones to create injection controlled media with close to homogeneous electric field profile. The physical reason for this approximate homogeneity is related to the blocking nature of the injected contact, which does not provide enough mobile carriers for developing of any electric field variation with a large gradient.

Processed samples were placed in waveguide-type sample holder, which enables to apply both microwave electric field and DC voltage bias. Microwave setup is presented in Fig. 6. By applying DC bias to the sample the changes in microwave transmission power are measured. To achieve very high DC electric field required

for Bloch gain, nanosecond DC voltage pulses were applied via transmission line technique. This enabled to observe high electric field induced microwave signatures with nanosecond time resolution.

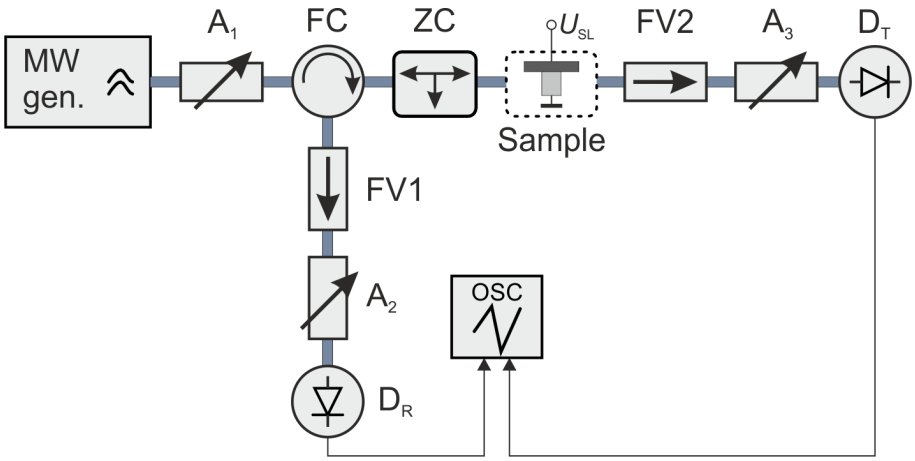

Figure 6. Setup for microwave measurements consisting of the following components: MW gen. - microwave generator, $A_{1,2,3}$ - precise microwave power attenuator, FC - ferrite circulator, FV1 and FV2 - ferrite valves, ZC - quarter wavelength impedance transformer, D_R and D_T - detectors for reflected and transmitted power measurement, OSC - digital oscilloscope.

The application of nanosecond pulses enabled to resolve four different physical processes occurring in the SL diode with applied bias voltage. It is illustrated via current, conductivity and transmission plots given in Fig. 7. It is seen that in region I (below 1 V) – the increase in current and conductivity is observed. The second part – voltage within 1–2.7 V, region II – exhibits peculiarity: increase of current becomes significantly slower, while conductivity experiences plateau. A peak appeared around 2.7 V can be attributed to the Zener tunneling via gap of 47 meV between the first and the second minibands of the SL. With further increase of voltage – within 2.7–4 V voltage range, region III – signatures of tunneling process between adjacent quantum wells becomes more pronounced, resulting in instability because of negative differential conductivity – voltage above 4 V (region IV. Hence, application of the voltage over the structure allows one to tune the SL via various working regimes. This is illustrated in Fig. 7c where microwave radiation experiences significant peculiarities with the variation of the forward bias voltage applied over the SL structure. One must note that microwave set-up is aligned so that reflection is kept to be minimal. Therefore, all the microwave transmission features can be attributed purely to the physical processes in the SL, but not to the change in the impedance matching/mismatching in a microwave circuitry.

As it is seen for the forward DC bias case at low voltages weak absorption signatures

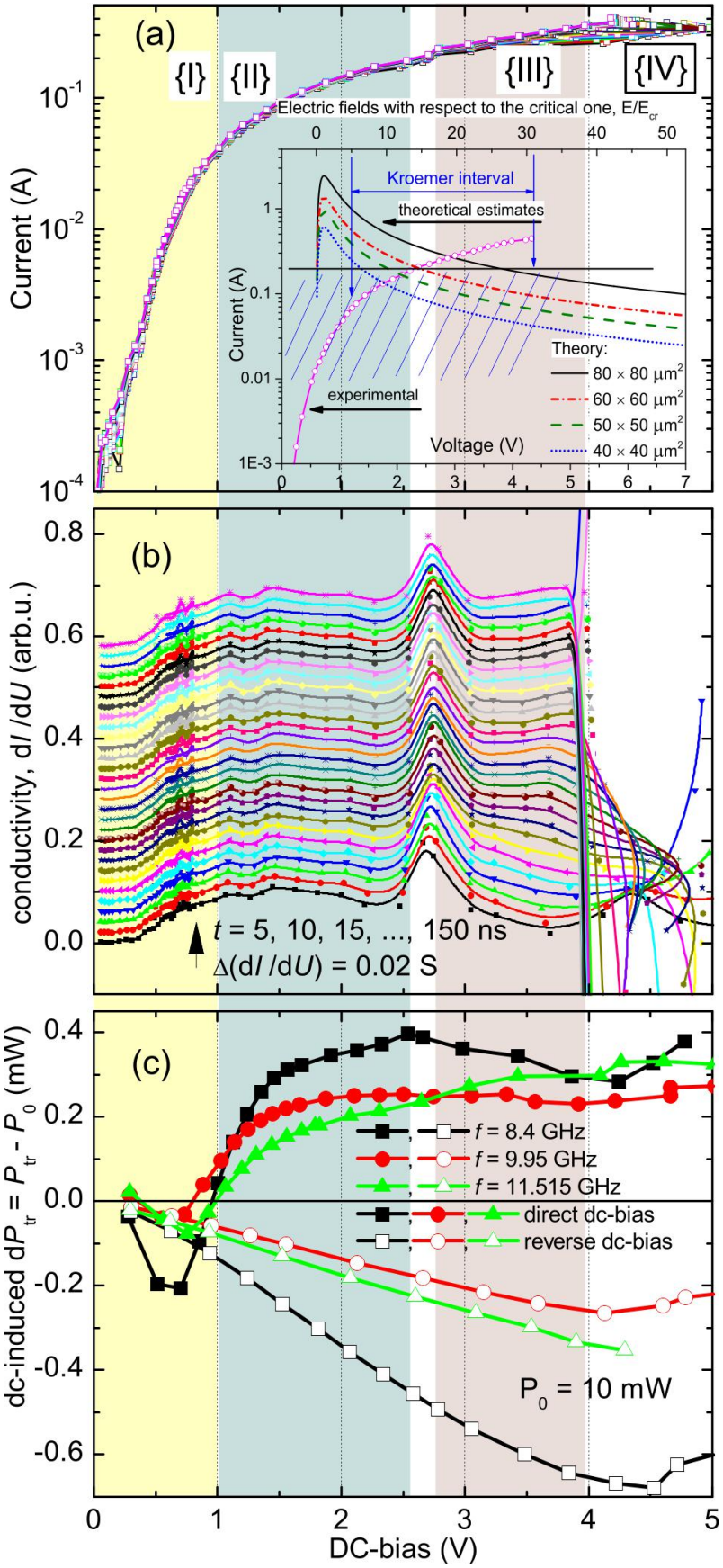

Figure 7. Current-voltage characteristics for GaAs/AlGaAs superlattice diode measured in time with 5 ns period (a). Inset shows calculated current characteristics using Esaki-Tsu model for different mesa dimensions. Conductivity dependence on voltage (b). Microwave power transmission difference induced by applied DC voltage (c).

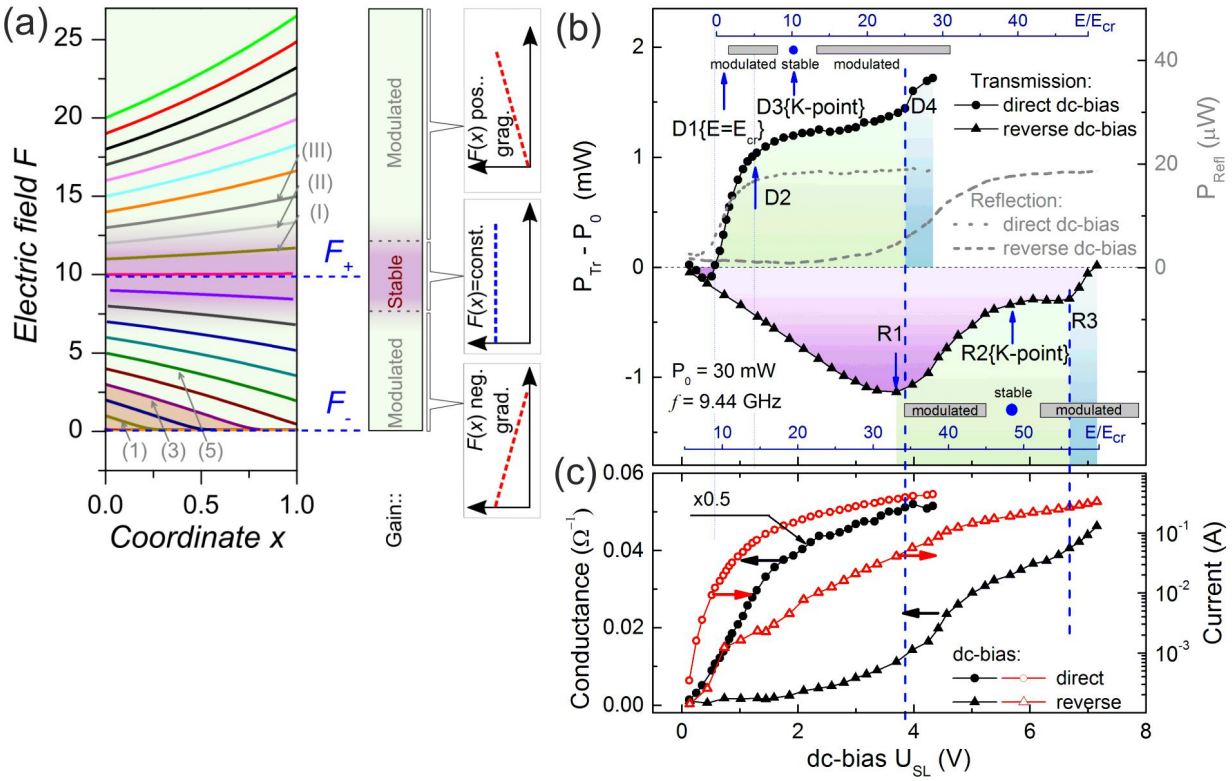

Figure 8. (a) Electric field spatial profiles in SL calculated by numerically solving 1 equation with different initial conditions $F(0)$. (b) Transmitted and reflected microwave power dependence on applied DC bias voltage. (c) Corresponding current-voltage characteristics shown in conductance and current scales.

are observed. With further increase of the applied voltage absorption disappears and the SL enters into the microwave gain area where DC bias induced transmission difference is positive. Whereas for the reverse DC bias no microwave gain is observed. Moreover, it is seen that microwave gain/absorption manifests strong correlation with the four regions aforesaid above.

To get more details in physical picture behind, we have performed analytical and numerical calculations by solving Poison and continuity equations for SL with drift velocity expressed as $v(F) = v_0 \frac{F}{1+F^2}$. differential equation for electric field spatial profile in SL can be written as (1), where $F = E/E_{cr}$ is electric field normalized to Esaki-Tsu critical field, $\tilde{x} = x/L$ – normalized coordinate, $J = j/(en_d v_0)$ - normalized current. Equation (1) has two stationary solutions (r.h.s $= 0$) expressed as 2, where electric field is the same and equal $F(0)$ through all SL length. F_+ point is always in the NDM region and it is called Kroemer point – here the electric field is uniform [15]. To reach it the electric field at the contact ($F(0)$) should be increased to a value equal to F_+. It also can be shown that for low current J case equation (1) has an analytical solution where electric field profile is close to homogeneous for large interval

of electric field values $F(0)$. In this work we call this interval – Kroemer interval. That is why to implement such low current regime GaAs/AlGaAs superlattice was placed between injection controlled contacts.

$$\frac{dF}{d\tilde{x}} = \alpha\left(\frac{J(1+F^2)}{F} - 1\right) \qquad (1) \qquad\qquad F_{\pm}(J) = \frac{1 \pm \sqrt{1-4J^2}}{2J} \qquad (2)$$

By numerically solving equation (1) electric field profiles were calculated. The results are displayed in Fig. 8a, where the electric field $F = E/E_{cr}$ is plotted as function of normalized coordinate x for different initial conditions $F(0)$. For SL to be tuned to amplification regime electric field should exceed Esaki-Tsu critical field E_{cr}. At low F values field profile has linear dependency with negative slope and amplification area covers only part of the SL. With further increase of the electric field, slope is decreasing and the amplification area extends over all the SL ($F = 5E_{cr}$). When electric field reaches $10E_{cr}$, Kroemer point F_+ is reached, and the electric field does not depend on the coordinate and becomes homogeneous within the whole SL length. The gradient of the electric field is zero here, and it continues to be small within a rather wide range of electric fields forming Kroemer interval. In such cases different type of Bloch gain may be observed. We will call it modulated Bloch gain, because of similarities with Bloch gain manifesting under excitation of modulated bias voltage [16].

Using aforegiven model, the results of microwave transmission measurements displayed in Fig. 8b were explained. For this reason electric field values corresponding to applied bias were calculated. Within the range of $0-5.4E_{cr}$ (1.3 V), drastic increase in gain is observed. Around 1.9 V corresponding to 10 E_{cr}, the gain is nearly independent of applied voltage, whilst in range of 15 E_{cr}– 27 E_{cr} it smoothly raises up. The existence of the plateau range is signature of the SL operating in stable Bloch gain regime. Wings around this region can be associated with the modulated Bloch gain: from the low-voltage side it is due to negative gradient of the electric field, while from the higher-one – because of the positive one. According to the theoretical predictions, the structure should be stable until the electric fields reach value of $31E_{cr}$. As it is seen from the experiment, instabilities are observed around $4\,\mathrm{V}//\sim 147\,\mathrm{kV/cm}//\sim 27E_{cr}$ – which is in reasonable agreement with theoretical estimates.

The situation becomes significantly different in the case of a deep barrier contact, for which current J is smaller, and, therefore, the position of the core, together with the embedded Kroemer point $F_+ = 1/J$, is shifted towards larger bias values (see

intervals in Fig. 4). Now the role of the left, low-voltage (depletion) wing of Kroemer interval in the transition to high frequency amplification drastically increases. In the far left of the wing, for which $F \ll F_+$, we have a complete depletion of the mobile carriers. Indeed, everywhere within Kroemer interval the scaled electron density $N = n/n_d$ is related to the bias F as $N = JF$, however, specifically in the case $F \ll F_+$, follows that $N \ll 1$. This strong depletion is accompanied by a relatively big negative values of the electric field gradient, which in turn require large values of F_{in} in order to realize the NDM regime in a sufficient part of the superlattice. Thus, for the deep barrier contact, not only the threshold voltage for amplification is larger, but also the coefficient of amplification is weaker. In the left wing of Kroemer interval (Fig. 8a), the mechanism of amplification is the modulated Bloch gain, for which an electron always spends some time in the low electric field state providing stable, but still weak high frequency gain. One can emphasize that this weak gain achieved in the superlattice often cannot overcome external losses arising in the whole device. This circumstance can explain the fact that in the case of reverse biased superlattice, the diode displays only decrease in absorption, but no net gain up to a rather large voltages.

To sum up results of this chapter, wide miniband GaAs/AlGaAs superlattice diode with injection-controlled contacts allows to create homogeneous electric field spatial profile in SL. It was demonstrated that stable electric field profile can be achieved within large interval of applied DC bias by extending Kroemer point to the Kroemer interval in the structure. By applying nanosecond pulsed DC bias signatures of Bloch gain in microwave frequency range were observed in room temperature experiment.

From the results presented in this chapter *the 2nd statement to defend* was formulated:

Asymmetric injecting/blocking contacts – Schottky contact and heterostructure - can be used to create homogeneous electric field in GaAs/AlGaAs superlattice within a range of applied bias voltage values. Under these conditions in strongly coupled GaAs/AlGaAs superlattice diode Bloch gain can be observed.

3 Terahertz radiation modes and their influence on terahertz imaging

Main criteria for selection of teraherz (THz) radiation source for imaging are based on emitted power and spatial beam profile. To achieve high imaging resolution either THz source operating in fundamental TEM_{00} mode should be used or beam profile correction should be employed. The latter technique adds additional power losses resulting in reduced signal-to-noise ratio of imaging system. On the other hand, single mode lasers usually emit lower power than multi-mode ones. Beam quality becomes especially important for compact THz sources, such as quantum cascade lasers (QCL). For instance QCL beam profiles have been thoroughly investigated [17] and plasmonic structures on the facets are developed for beam profile correction. However, as far as we know, there are no works aiming to study how imperfect beam profile affects THz imaging quality. Therefore this chapter of the thesis is dedicated to the investigation of THz imaging system based on multimode laser source.

In this experiment commercial continuous wave THz laser (FIRL-100, Edinburgh Instruments) providing a well-defined TEM01 beam was used. The setup for reflection imaging system is shown in Fig. 9.

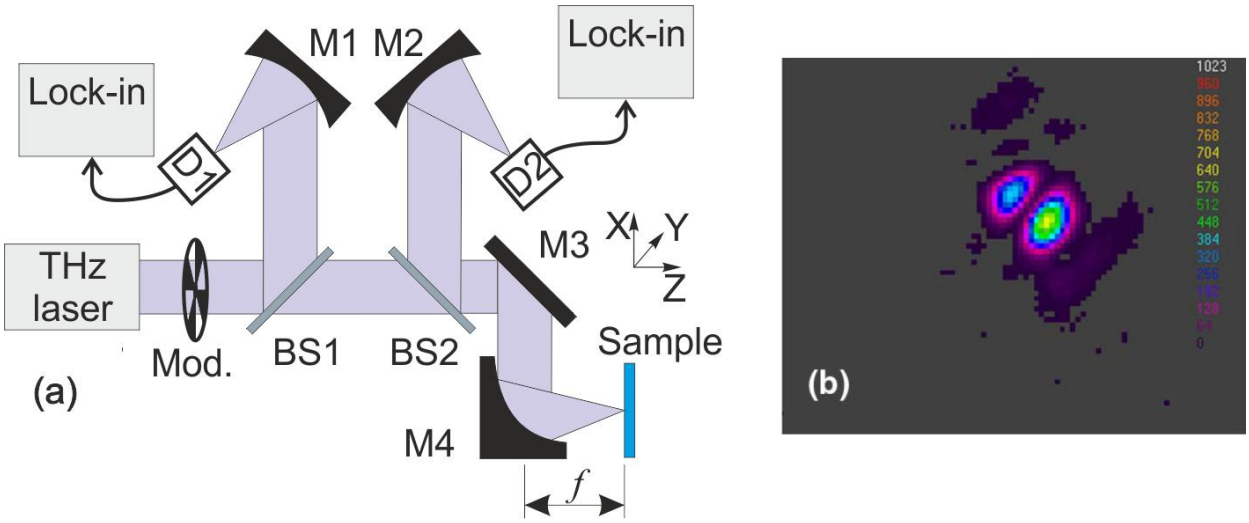

Figure 9. (a) THz imaging setup for reflectance measurements. (b) Measured beam profile of laser TEM_{01} mode.

The laser beam is divided into two parts by the beam splitter BS1. Reflected part is directed to detector D1 for laser output power monitoring. The transmitted part was used for reflectance measurements of the sample placed in the focal plane of the off-axis parabolic mirror M4. Radiation reflected from the sample is collected with the same mirror M4 and guided to the detector D2 by means of additional

beam splitter BS2 and spherical mirror M2. Imaging performance of the system was studied by replacing M4 with focusing mirrors of different focal lengths. The sample was always kept in the focal plane of the focusing mirror. Three mirrors with diameter of $D = 5\,\mathrm{cm}$, but different focal length f of 5, 10, and 15 cm, were used for the experiments.

The THz radiation was modulated by mechanical modulator and measured with large aperture (9 mm) pyroelectric detectors D1 and D2 using lock-in amplifiers. Detector signals were recorded synchronously with the sample movement. The sample was placed on a two-axis (XY-plane) translation stage and was raster scanned at a constant speed up to 300 mm/s in the X axis direction and with fixed size steps in the Y axis. Frequency of amplitude modulation and integration time constant of the lock-in amplifier were 235 Hz and 10 ms, respectively. Pyroelectric detectors D1 and D2 were placed in the focal plane of the spherical mirror M1 and M2, respectively, to ensure that the entire laser beam was measured without any spatial modes filtering. Depending on size and resolution it took 5–15 min. to scan one THz image.

For the experiment THz laser was tuned to the frequency of 2.52 THz providing well defined first-order Hermite–Gaussian (TEM_{01}) mode shown in Fig. 9b. The maximum emitted power was 20 mW and beam size of $w = 30\,\mathrm{mm}$ was measured at $1/e^2$ level.

Performance of THz imaging system was evaluated using specially made high resolution target, so called "Siemens star". The target was fabricated by using direct laser writing technique[3] from metalized silicon wafer. A photo of the fabricated target is shown in Fig. 9(b). The target was patterned with 18 equal trapezium rays equidistantly displaced in a full circle. The width of each trapezium increases from 75 to 1750 µm going outward from the center. The diameter of central metal circle was about 860 µm. Some open areas were additionally processed to reduce THz reflectance by forming black silicon [18] visible as black areas in the photo.

THz images of the “Siemens star” recorded with the multimode laser beam using different focal length mirrors are shown in Fig. 10. In the case of the largest focal length mirror of 15 cm patterns of the target appeared doubled and blurred (Fig. 9a). Misrepresentations were already smaller for the case of $f = 10\,\mathrm{cm}$ (Fig. 10b) still preserved in the central part of the image and they became almost invisible using the mirror with $f = 5\,\mathrm{cm}$ (Fig. 10c). To prove that misrepresentation of THz images occurred due to multi mode beam profile additional image were taken for the case $f = 15\,\mathrm{cm}$ with detector aperture limited to 1 mm. This ensured that only one lobe

[3]High resolution target was fabricated by B. Voisiat, Center for Physical Science and Technology, Lithuania.

of TEM_{01} is measured. As a result blurring and doubling effects were not visible (Fig. 10d) with spatial mode filtering applied. The same result may be achieved by using $f = 5\,\text{cm}$ mirror together with multi mode laser beam.

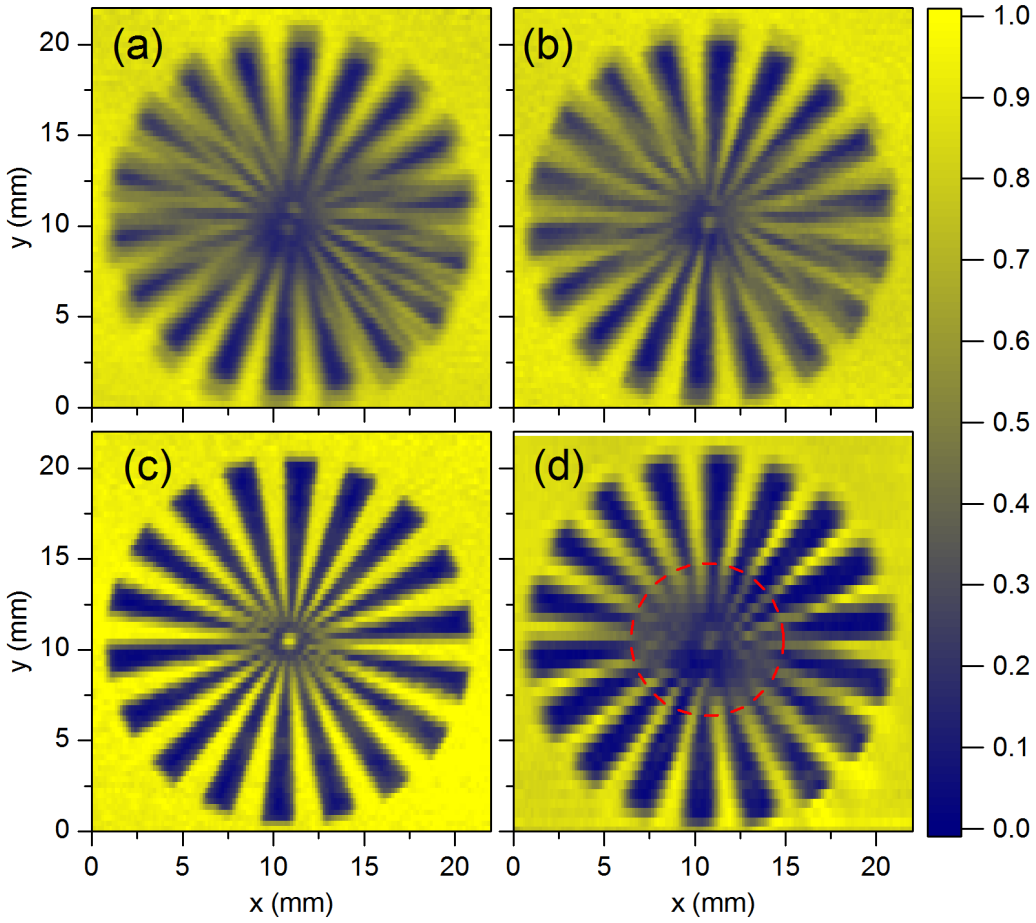

Figure 10. Terahertz reflectance images of "Siemens star" target measured using different focal length f parabolic mirrors: (a) and (d) – $f = 15\,\text{cm}$, (b) – $f = 10\,\text{cm}$, (c) – $f = 5\,\text{cm}$. Image in section (d) was measured with detector aperture limited by pinhole to 1 mm. Red line corresponds to Rayleigh circle with radius $r_R = 42\,\text{mm}$. [A3]

To evaluate maximum resolution of the system imaging for the case $f = 5\,\text{cm}$ was repeated using slower scan velocity (Fig. 11). In this case only minor blurring occurs around the edges of the center circle. More detailed analysis of the image revealed that patterns as small as $100\,\mu\text{m}$ can be distinguished via THz imaging with TEM_{01} mode. This corresponds to the resolution of 0.84λ. Also areas with black silicon are visible, where measured reflectance was less than 1 %.

Resolution of imaging systems can be estimated by Rayleigh length criterion $l = 1.22\lambda f/D$. In this work for the "Siemens star" target it is more convenient to use Rayleigh circle criterion with its radius r_R defined as $r_R = \frac{1.22\lambda N f}{\pi D}$. Here λ is wavelength, N – number of rays, f –focal length, and D is diameter of radiation beam. Rayleigh

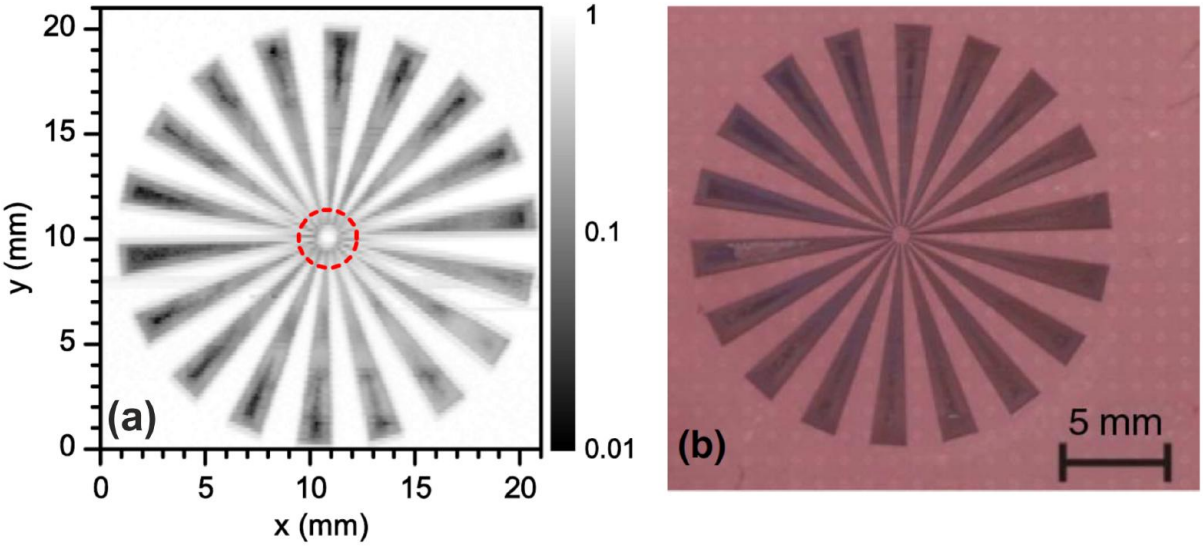

Figure 11. (a) High resolution THz reflectance image of "Siemens star" target measured with $f = 5\,\text{cm}$ mirror. Red line marks Rayleigh circle with radius $r_R = 1.4\,\text{mm}$. (b) Photo of high resolution target "Siemens star". [A3]

radius corresponds to a distance between the center and a point where the width of trapeziums is equal to Rayleigh length. Using $N = 18$ and numerical aperture values $NA = D/f = 0.6,\ 0.3$ and 0.2 Rayleigh radius of $r_R = 1.4,\ 2.8,$ and $4.2\,\text{mm}$ was calculated for the focal length of $5,\ 10,$ and $15\,\text{cm}$.

Using Rayleigh circle it was possible to describe the imaging system based on the single-mode (Fig. 10d) and the multimode lasers (Fig. 11) but with the $0.6\,\text{NA}$ focusing mirror only. The multimode laser system with smaller numerical aperture focusing mirrors was not efficient in terms of subwavelength resolution imaging since the blurring effects extended beyond the Rayleigh circle. In this case, r_R should be multiplied by 2 because of increased beam width in the focal spot [19].

Designed THz imaging system with multimode laser source and correctly selected optics was applied for solar cell imaging Fig. 12. It is worth noting that due to high resolution, THz imaging allowed to inspect tab and finger wire defects.

To sum up, TEM_{01} laser mode was successfully applied for high resolution THz imaging at the radiation frequency of $2.52\,\text{THz}$. High resolution target is patterned in $75\,\mu\text{m}$ scale. It was shown that by using short focal length parabolic mirror imaging resolution is limited by diffraction limit and not by the beam profile quality. TEM_{01} laser mode was successfully applied for investigation of solar cell contacts.

From the results presented in this chapter *the 3rd statement to defend* was formulated:

The use of focusing optics with short focal distance in the imaging system with a radiation source emitting TEM_{01} beam mode of terahertz radiation allows one to

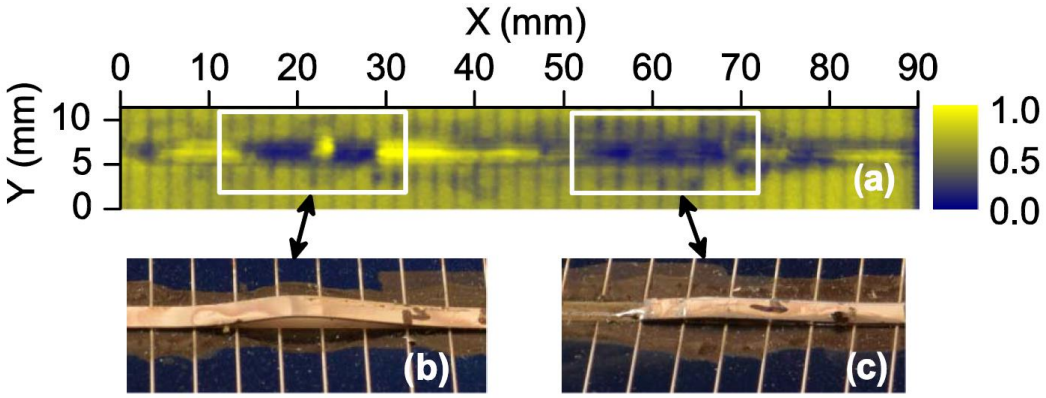

Figure 12. THz reflectance image (a) of silicon solar cell measured at 2.52 THz frequency using $f = 10\,\text{cm}$ (NA $= 0.3$) focusing mirror. Image consists of 300×38 pixels with pixel size being $300 \times 300\,\mu\text{m}^2$, acquisition time is about 12 min. White line marks contact defects shown in photos (b) and (c). [A3]

record good quality terahertz images with spatial resolution close to the diffraction limit.

4 Application of compact non-coherent detectors for spectroscopic terahertz imaging systems

Terahertz radiation (THz) is well known for its ability to propagate through non-conducting substances including common packaging materials. This provides a possibility to screen objects inside package via active THz imaging [20]. Because of many organic materials, including drugs, explosives, chemical and biological agents, exhibit characteristic spectral signatures in THz range [21], special attention is paid for spectroscopic THz imaging systems capable to reveal and inspect potentially dangerous materials.

Implementation of such THz systems may be based on spectroscopic THz imaging [1] combined with a principal component analysis (PCA) [22] allowing qualitative discrimination of materials if their spectra are *a priori* known. Practical application of such systems requires not only high sensitivity, low-noise and higher dynamic range of the sensing components – key features become speed, stability and robustness as well as wide bandwidth operation. Therefore, this chapter is dedicated to the investigation and application of innovative non-coherent THz detectors such as InGaAs bow-tie (BT) diodes, CMOS field effect transistors (TeraFET) and Ti microbolometers for spectroscopic THz imaging systems.

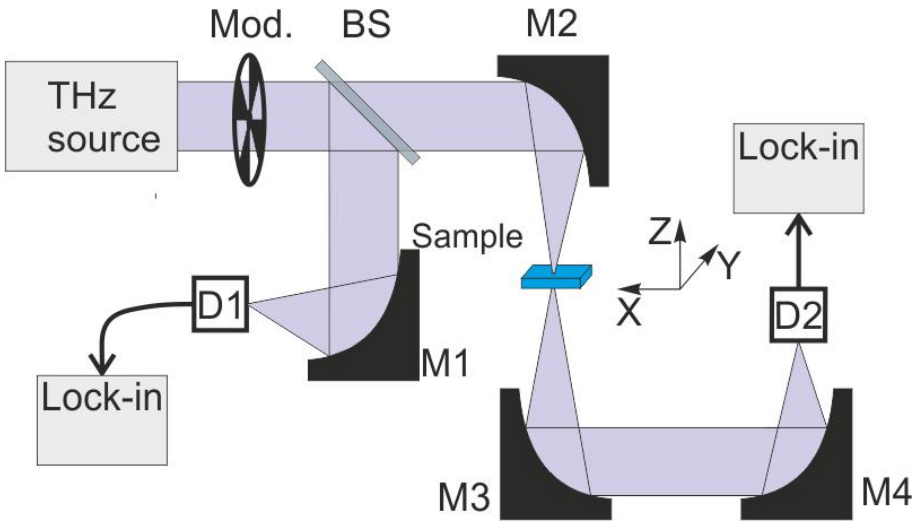

Figure 13. Spectroscopic THz imaging system in transmission geometry.

Typical experimental setup for spectroscopic THz transmission imaging is presented in Fig. 13. THz radiation emitted by optically pumped molecular THz laser (FIRL-1000) is used to measure sample transmittance. Detector D1 is used to monitor changes in laser power. Sample under investigation is placed in the focal plane between two off-axis parabolic mirrors. THz radiation transmitted through sample

is measured with THz detector D2. Signals of detectors are measured with lock-in amplifiers. Experiment is carried out at room temperature.

To acquire 2D transmission images sample is raster scanned in XY plane using fast position synchronized measurement ($dx = 0.1\,\mathrm{mm}$) while positioning stage moves with constant velocity in X axis direction and stepped motion in Y axis direction ($dy = 0.3\,\mathrm{mm}$).

To test spectroscopic imaging systems with different detectors special samples were prepared. As one of the most attractive applications of spectroscopic imaging is in security systems, instead of real explosive materials, for the safety reasons, explosive imitators should be used. It is known that in THz range sucrose (SC) and tartaric acid (TA) display spectral lines similar to PETN and RDX, respectively [23].

Therefore, to demonstrate spectroscopic imaging possibilities a number of pellets were prepared containing different materials such as lactic acid (LA), tartaric acid (TA) and sucrose (SC). For the LA, we used commercially available medicine pellet. As TA and SC materials are highly absorbing THz radiation, only small concentration mixtures with PTFE (Polytetrafluoroethylene) were found suited for experiments. Four sample mixtures were made containing 10% TA, 10% SC, 5% TA-5% SC, and 100% PTFE. Under application of pressure, pellets of $1.4\,\mathrm{mm}$ thickness and $13\,\mathrm{mm}$ diameter were formed from powder mixture.

Principal component analysis requires material spectra to be *a priori* known. Therefore transmittance spectra were measured for TA, SC and PTFE samples with custom Fourier transform spectrometer. Spectrum of LA pellet was measured via THz Time-Domain spectroscopy. Results are shown in Fig. 14 in a form of transmittance and absorbance $-ln(T)$. As it is seen, LA has significant absorption line at 0.54 THz. TA and SC displays spectral signatures within range $0.6-4.5\,\mathrm{THz}$. THz laser frequency lines used in experiment are marked by arrows in Fig. 14a. One can see that for qualitative identification between 10%TA and 10%SC the most suited frequency lines are $0.762\,\mathrm{THz}$ and $1.840\,\mathrm{THz}$, because transmittance differs 2 and 4 times, respectively. It is worth noting that at $2.52\,\mathrm{THz}$ transmittance difference amounts to only 20%.

4.1 Spectroscopic imaging with InGaAs bow-tie diodes for frequencies up to 2.52 THz

Detection of THz radiation with asymmetrically shaped 2D electron layers was suggested in works [24, 25]. However, sensitivity was determined to be around $0.3\,\mathrm{V/W}$, therefore, application of such detectors for spectroscopic imaging is complicated as

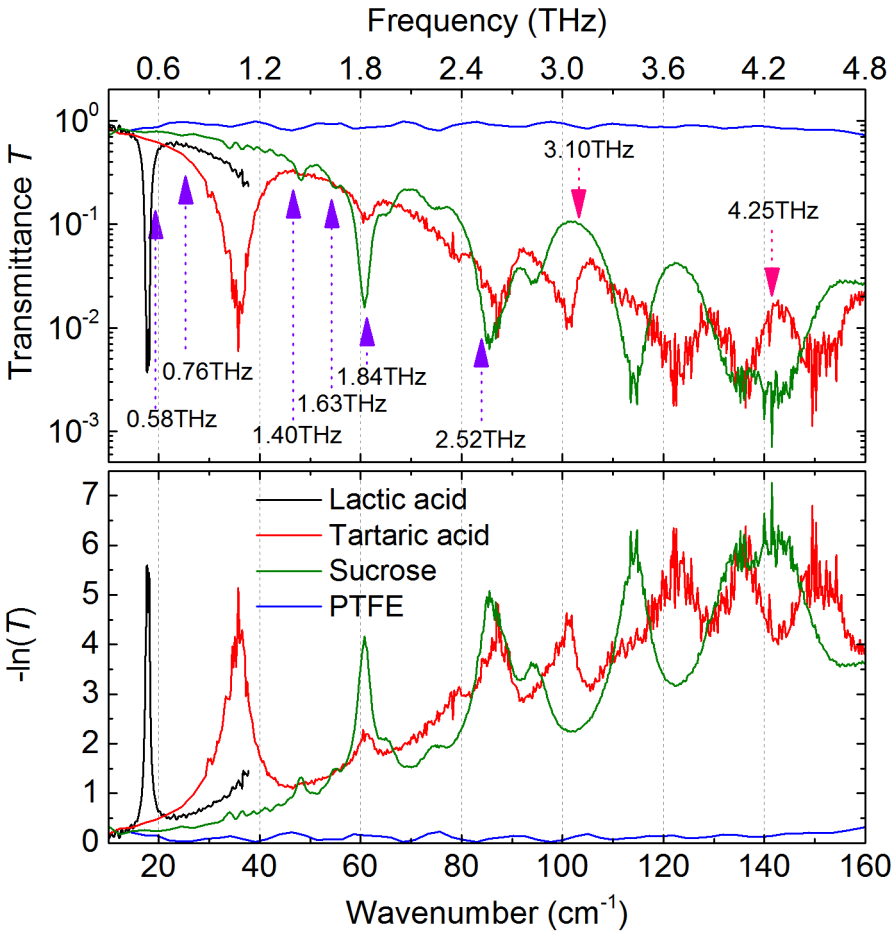

Figure 14. Transmittance T (a) and $-ln(T)$ (b) spectra of pellets made from lactic acid (LA), tartaric acid (10% TA), sucrose (10% SC) and 100% PTFE.

higher sensitivity is needed. Because the detection principle is based on carrier heating, the sensitivity can be increased by selecting proper materials with higher mobility.

In this experiment wide bandwidth detector based on asymmetrically shaped (bow-tie, BT) InGaAs diode [26] was used. Schematic design of the detector is shown in Fig. 15. The diode was fabricated from $In_{0.54}Ga_{0.46}As/InP$ heterostructure with 2DEG layer which electron concentration and mobility are about $2 \times 10^{15}\,\mathrm{cm}^{-3}$ and $13\,300\,\mathrm{cm}^2/\mathrm{Vs}$, respectively. The device was designed as bow-tie antenna with one of two semiconductor leaves being metalized. Active area was formed by etching $3\,\mu\mathrm{m}$ height mesa. Detector dimensions are: $d = 12\,\mu\mathrm{m}$, $a = 50\,\mu\mathrm{m}$, $l = 250\,\mu\mathrm{m}$,$L = 500\,\mu\mathrm{m}$ ir $w = 100\,\mu\mathrm{m}$. The diode was attached to a hemispherical $6\,\mathrm{mm}$ diameter silicon lens for effective coupling of incident radiation. Important parameter is detector response time, which is found to be less than $7\,\mathrm{ns}$ [27].

It worth noticing that unlike nanometer field effect transistors, BT diode detector has dimensions of µm. Therefore, it exhibits reasonable reliability to electrostatic

discharge and high incident power of microwave-THz radiation [27].

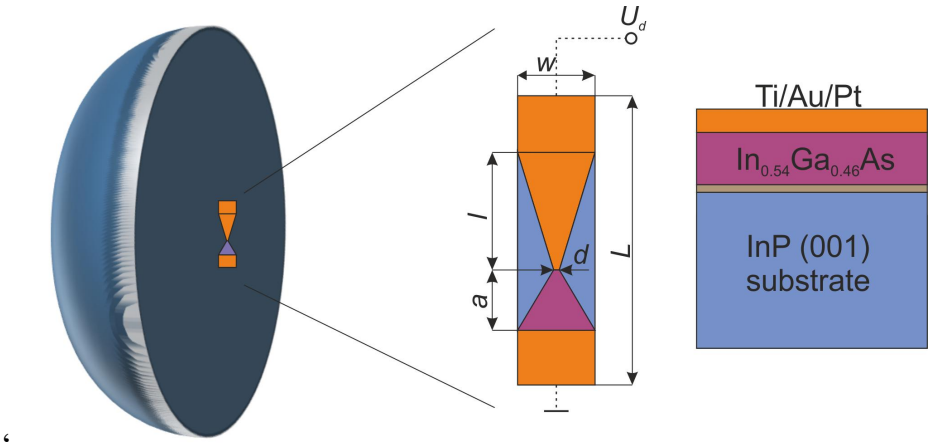

Figure 15. InGaAs bow-tie diode detector coupled with silicon lens: (a) - schematic view; (b) - diode structure and dimensions; (c) - design of InGaAs/InP heterostructure used for detector fabrication.

InGaAs bow-tie diode was applied for spectroscopic THz imaging. For that reason optimal working conditions were found by measuring detector sensitivity at 0.762 THz and noise voltage dependencies on DC bias current. As it is shown in Fig. 16 the sensitivity increased by about 20% after application of reverse current of only in the range of 3 µA. However, at the same time detector noise also increases. The noise equivalent value (NEP) of the device was calculated as a ratio between the noise voltage and the sensitivity. The sensitivity of the BT diode was found to be of about 10 V/W and an unbiased connection provided the lowest NEP value of about 5.8 nW/$\sqrt{\text{Hz}}$.

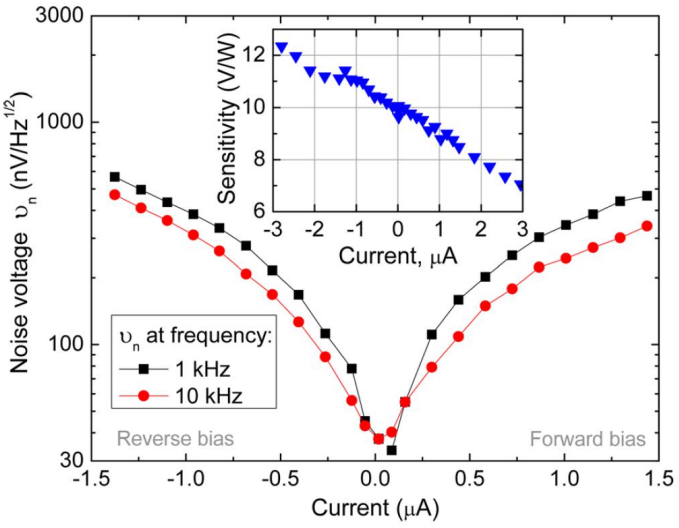

Figure 16. Sensitivity and noise voltage dependencies on DC bias current for InGaAs bow-tie diode. [A4]

Using InGaAs BT diodes pellets framed in metallic holder were imaged at discrete 0.585, 0.762, 1.40, 1.63, 1.84, and 2.52 THz THz laser frequencies. Results are shown in Fig. 17.

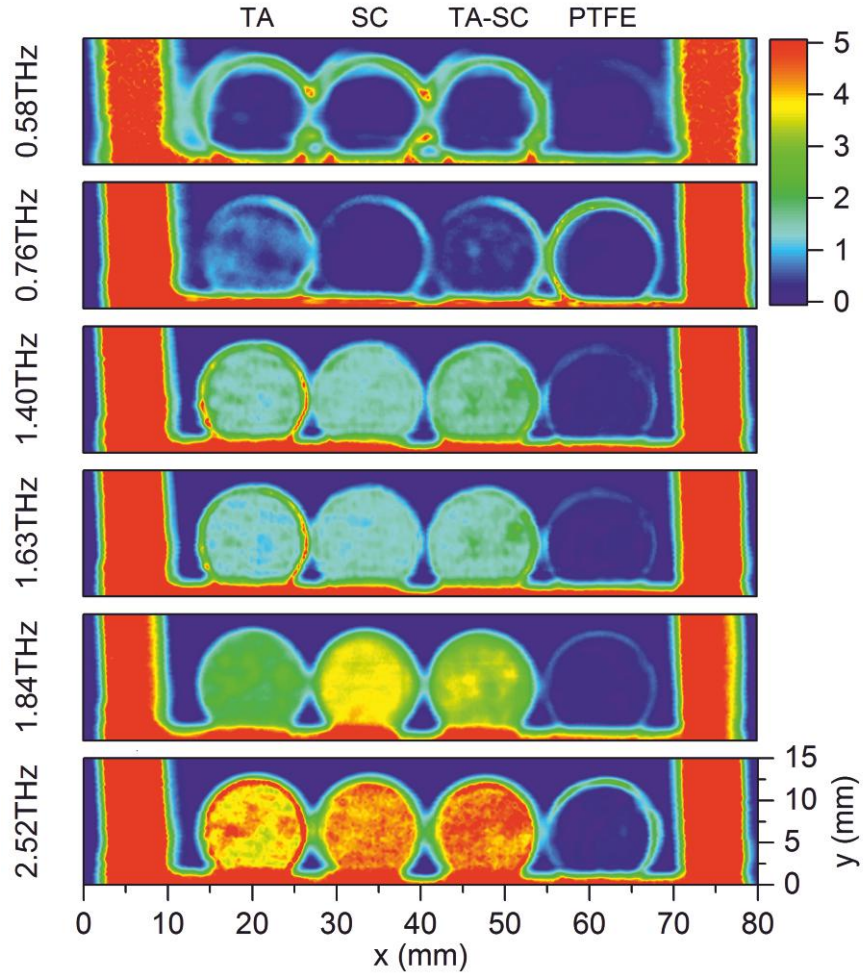

Figure 17. THz absorbance ($-ln(T)$) images of TA, SC, TA-SC and PTFE pellets taken at different THz frequencies. [A2]

Images were obtained by measuring sample transmittance T and calculating absorbance $-\lg T$. It is seen that at frequencies 0.58, 1.40 and 1.63 THz, absorbance of TA and SC is similar. However, images at frequencies 0.76, 1.84 and 2.52 THz samples differs strongly. By comparing average absorbance values measured via spectroscopic imaging and Fourier transform spectrometer data good agreement between the results was indicated. Signal-to-noise ratio of the system was found to be no less than 300. Imaging results show inhomogeneous absorbance distribution in the pellets because of inhomogeneous material distribution in pellets.

More precise distribution of materials in the samples was estimated using PCA by

solving overdetermined system of linear equations

$$Z_{N,M} \cdot X_M = Y_N, \tag{3}$$

where $Z_{N,M}$ is coefficient matrix composed of sucrose and tartaric acid absorption values ($M = 2$) measured by Fourier transform spectroscopy (or *a priori* known), and Y_N is spatial map of absorbance measured by the spectroscopic THz imaging system at $N = 6$ frequencies. The component map X_M was found performing a standard least squares fit. Found admixtures map is shown in Fig. 18. The range of interest of square area fitted into the pellet was taken into consideration and the mean and standard deviation values were calculated. The results were summarized in Table 1. One can see that the BT diode-based spectroscopic THz imaging system provides reasonably good accuracy data consistent with initial concentrations of SC and TA used for preparation of pellets.

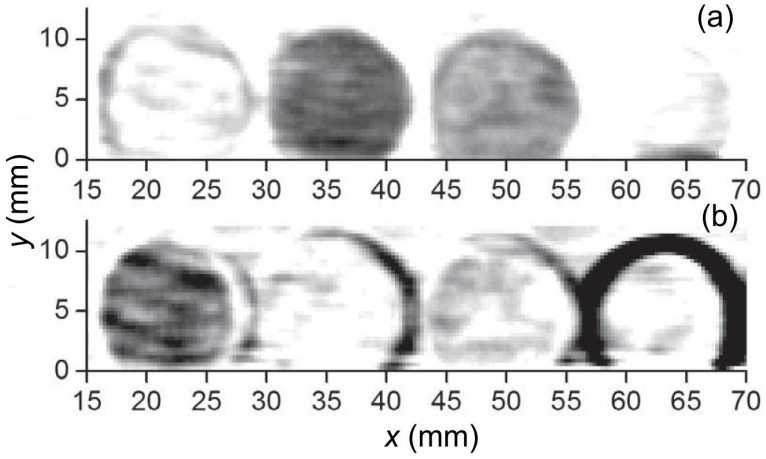

Figure 18. Sucrose (a) and tartaric acid (b) distribution in the samples. Dark color corresponds to higher concentration, white - to lower. [A2]

Table 1. Sucrose and tartaric acid concentration in the samples measured via spectroscopic imaging.

Component	Nr. 1	Nr. 2	Nr. 3	Nr. 4
Sucrose (%)	0.1 ± 1.1	0.0 ± 0.9	6.1 ± 0.8	-0.3 ± 0.9
Tartaric acid (%)	9.9 ± 0.7	10.1 ± 1.4	2.5 ± 1.3	0.3 ± 1.4

Spectroscopic imaging experiment was also repeated for the samples enclosed in HDPE box. Similar results were acquired. Data can be found in [A2] publication.

Spectroscopic THz imaging systems with InGaAs BT diodes operated reasonable in the frequency range up to 2.52 THz. High frequency limit is defined by the bandwith of detector. Sensitivity dependence on frequency for the diodes produced of

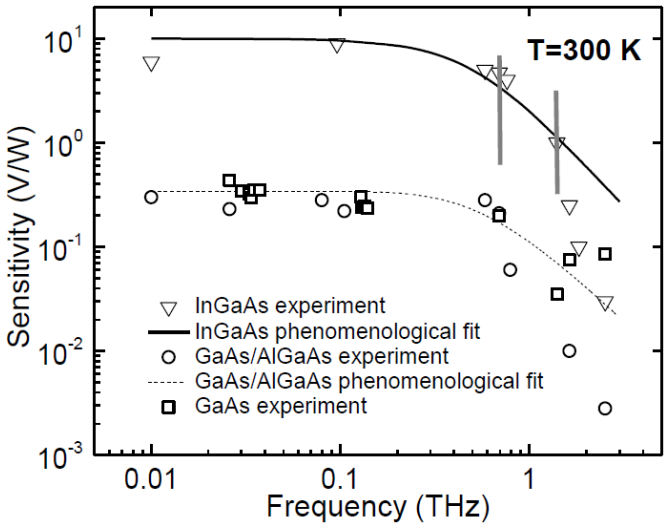

Figure 19. Frequency dependence of sensitivity for bow-tie diodes fabricated from InGaAs, GaAs/AlGaAs [24] ir GaAs [28]. [B1]

different materials is shown in Fig. 19. Up to 1 THz sensitivity varies weakly and it is about 10 V/W. Above 1 THz sensitivity drops drastically because of momentum relaxation time and reduced efficiency of antenna coupling [26]. Frequency range for spectroscopic imaging can be extended using plasmonic mixing phenomena in nanometric field effect transistors.

4.2 Spectroscopic imaging with field effect transistors

Nanometric field effect transistors (TeraFET) intended for sensitive detection of THz radiation were designed by prof. H. Roskos group in J.W. Goethe university (Frankfurt/M, Germany). Resonant patch antenna coupled TeraFETs were manufactured by commercial 90 nm CMOS technology. The detectors were specifically designed to be resonant at molecular THz laser frequency lines: 2.52 THz, 3.18 THz and 4.25 THz. Different frequency detectors were manufactured as multicolor array on single chip which was connected to compact microcircuit with a possibility to change active detector. More detailed information about TeraFET detectors can be found in work by A. Lisauskas *et al.* [29].

At the first stage of experiment sensitivity and NEP of the detectors were measured. Obtained results are shown in Table 2.

TeraFET detectors were employed for spectroscopic THz imaging of the same samples as in the previous section. Transmission images of pellets were recorded at 0.7619, 1.8397, 2.5242, 3.1075, ir 4.2475 THz frequencies. Frequencies of 0.7619 and 1.8397 THz were detected by additional sensors with antenna-resonant frequen-

Table 2. Sensitivity and noise equivalent power (NEP) for TeraFET detectors.

Frequency (THz)	Sensitivity (V/W)	NEP(pW/$\sqrt{(}$Hz))
2.52	336	63
3.12	308	85
4.25	230	110

cies near the laser lines, 0.648 ir 1.63 THz, respectively. Despite of small detuning, their performance was found to be sufficient enough for THz imaging. More details on these detectors are available in Ref. [A1].

THz images were recorded with spectroscopic imaging setup presented in Fig. 13. Measured THz images are shown in Fig. 20. Images at different frequencies were taken by changing THz laser line and switching to appropriate detector to selected frequency. After each change, the detector position was adjusted to maximize the signal. Recorded images display dynamic range of 22 dB and for some cases even more. Only in the case of 1.84 THz increased noise level was present resulting in smaller dynamic range of 18 dB because of discrepancy between the laser line and the detector resonant frequencies.

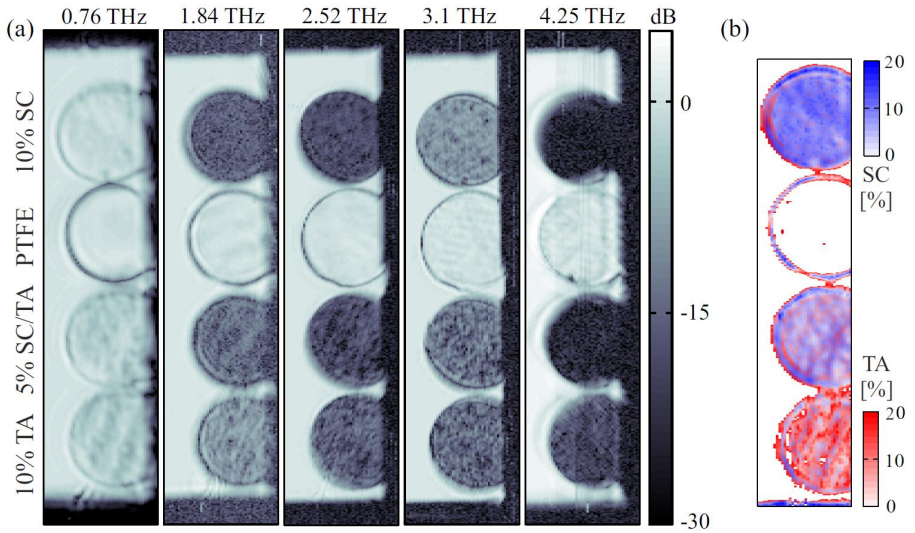

Figure 20. (a) Spectroscopic transmission images of explosive imitators measured with resonant TeraFET detectors. (b) Calculated spatial distribution of sucrose (SC) and tartaric acid (TA) concentrations in the samples. [A1]

More detailed analysis of images were carried out by calculating average transmission values for each pellet at different frequencies. Obtained values were compared with Fourier transform data (Fig. 3). Good agreement is evidenced.

Spectroscopic imaging allows one to determine admixture distribution in sample. By using PCA (3) distribution of sucrose and tartaric acid was found (Fig. 20b). As

Table 3. Transmittance values of explosive imitators measured with TeraFET detectors and Fourier transform spectroscopy (FTIR). [A1]

	TeraFETs				FTIR			
f [THz]	10% TA	MIX	PTFE	10% SC	10% TA	MIX	PTFE	10% SC
0.76	0.489	0.573	1	0.772	0.410	0.488	0.798	0.724
1.84	0.130	0.046	1	0.030	0.133	0.048	0.838	0.028
2.52	0.030	0.017	1	0.017	0.038	0.021	0.858	0.017
3.1	0.040	0.052	1	0.116	0.038	0.051	0.844	0.118
4.25	0.015	0.006	1	0.004	0.022	0.009	0.792	0.002

it is seen, concentration of components is distributed inhomogeneously in the samples which is consistent with the results obtained by using InGaAs BT diodes presented in previous section.

4.3 Application of microbolometer detectors for spectroscopic imaging system with optoelectronic THz emitters

Terahertz time-domain spectroscopic systems (THz-TDS) are widely used for spectral measurements and imaging in room temperature conditions with higher than 60 dB dynamic range in wide frequency range [30]. However, coherent detection used THz-TDS systems enables high sensitivity, but are complex and relatively slow in recording image in two-dimensions. For direct practical applications one needs faster and more compact systems. As a solution for such issues non-coherent detectors could be employed for the detection of THz radiation emitted from optoelectronic emitter. Such configuration displays advantages such as an increased performance speed because measurement of pulse time dependence is no longer necessary. It simplifies the systems and reduces price because of no needs to guide optical probe pulses to the detector through mechanical delay line, which is also not needed in such configuration. However, to proceed in this direction very sensitive detectors are required because of low average power of optoelectronic emitters.

In the following section of this work resonant antenna-coupled titanium microbolometers are applied for the detection of THz radiation emitted from optoelectronic emitter. Detector were fabricated by prof. J. Trontelj group in University of Ljubljana, Slovenia. Microbolometers were optimized according to criteria such as high temperature coefficient, low noise, manufacturing process is compatible with commercial silicon technology, long-term stability. Design and photo taken by electron microscope of optimized titanium microbolometer are shown in Fig. 21. More details

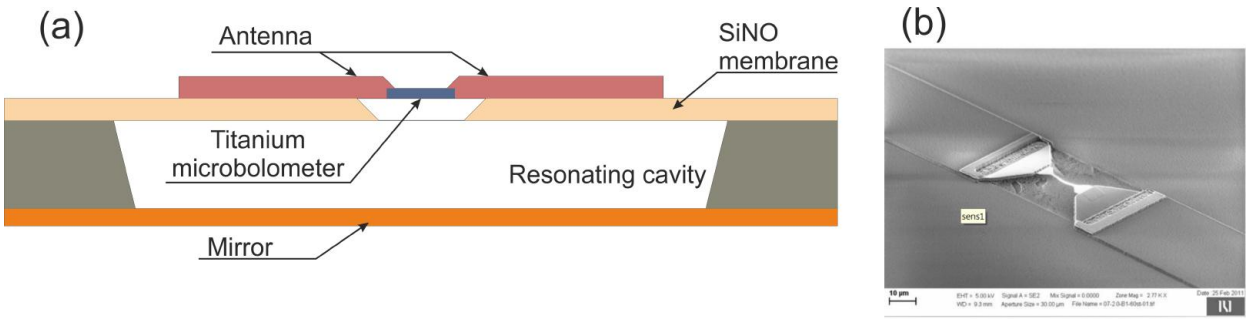

Figure 21. Cross-section view (a) and SEM photo (b) of Ti microbolometer detector. [31]

about Ti microbolometer detectors can be found in Ref. [31].

In this work, detectors designed for resonant frequencies of 0.3 THz (LV3) and 0.6 THz (LV6) were selected. Detectors were integrated into microcircuits with low noise amplifiers. Its basic characteristics are: response time less than 1 µs, sensitivity up to 300 V/W and NEP below 14 $\mathrm{pW}/\sqrt{\mathrm{Hz}}$.

High sensitivity and low NEP allowed to measure response spectra with Fourier transform spectrometer. Result are shown in Fig. 22. In case of LV3 detector (Fig. 22a) antenna gain characteristic calculated via ANSYS HFSS software packet[4] is also plotted. Experimental results show good agreement with calculated data. For the LV6 detector (Fig. 22b) two peaks are observed. The first one is related to the resonant frequency of 0.6 GHz, whilst another side peak, at 1.3 THz, is probably observed due to not optimal resonator. Note that other optimized detector do not exhibit such peak. For further experiments presented in this section, side peak influences on results negligibly, because the power of optoelectronic source and transmittance of the samples drops significantly in the frequency range above 1 THz.

Spectroscopic imaging was carried out using Titanium microbolometers in equivalent imaging system as presented in Fig. 13. As THz source served LTG-GaAs photoconductive antenna emitter, excited with femtosecond optical pulses generated by Titanium:saphire laser. The emitter generates wide bandwidth radiation of 1.2 µW average power. Due to the wide bandwidth operation of the emitter frequency selectivity required for spectroscopic THz imaging was obtained by resonant antennas coupled with microbolometers.

To test proposed spectroscopic THz imaging system pellets containing lactose acid (LA), and tartaric acid (TA) were imaged using LV3 and LV6 microbolometer detectors. Samples were enclosed in high density polyethylene (HDPE) box as it is shown in Fig. 23a. Measured THz images are displayed in Fig. 23b-c.

Pellets containing LA and TA exhibit different transmittance in the images taken

[4]Calculations were carried out in Ljubljana university.

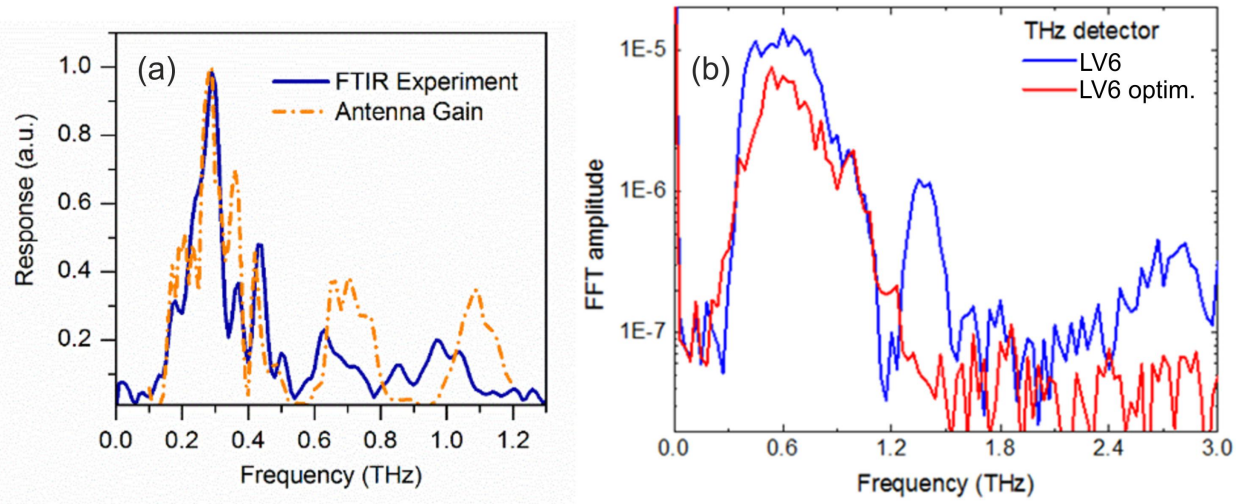

Figure 22. Response spectra of microbolometer detectors LV3 (a) and LV6 (b) with resonant frequency at 300 GHz and 600 GHz, respectively, measured with Fourier spectrometer. For LV3 case calculated antenna gain is presented. [C4]

with LV3 and LV7 detectors. Transmittance spectra obtained via Fourier transform spectroscopy LA and TA were used to estimate distribution by solving 3 equations (Fig. 23d-e). As it is seen, the highest LA concentration was observed in pellet 1 (lighter color), whereas highest TA concentration was found in pellet 2.

Experimental results prove that Ti microbolometers can be used to record high quality images in spectroscopic THz imaging systems with optoelectronic emitters. The THz imaging system presented in this section was published in Lithuanian patent *IMAGING SYSTEM OF TERAHERTZ FREQUENCY BAND* [B2].

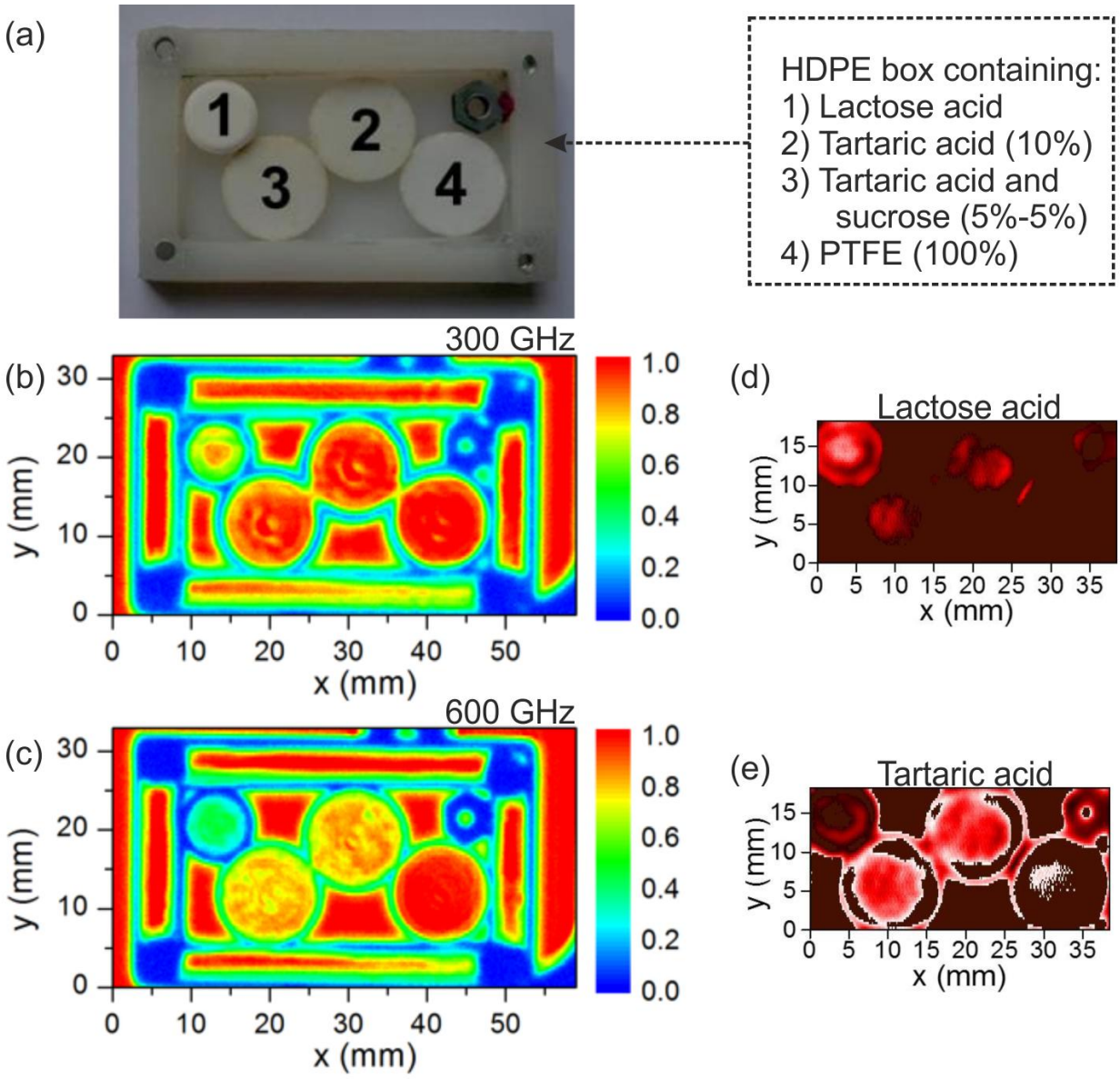

Figure 23. Photo of the samples placed in HDPE box (a); THz images of the samples measured with LV3 (b) and LV6 (c) microbolometer detectors; lactose acid (d) and tartaric acid (e) distribution calculated via principal component analysis. [C4]

Chapter summary

In this chapter innovative compact room temperature THz detectors were applied for spectroscopic imaging systems working in direct detection mode. InGaAs bow-tie diode detectors were used for THz imaging and principal compositional analysis of samples containing sucrose and tartaric acid in the frequency range from 0.5 to 2.5 THz. Frequency range for spectroscopic imaging was extended up to 4.25 THz by using antenna coupled CMOS field effect transistors employing plasmonic mixing for THz detection. Antenna coupled titanium microbolometers were applied in spectroscopic imaging system based on small average power optoelectronic emitter. It was demonstrated that small NEP value in order of $10\,\mathrm{pW}/\sqrt{\mathrm{Hz}}$ of such devices is sufficient for the detection of THz radiation emitted by optoelectronic emitters in spectroscopic imaging system.

From the results presented in this chapter *4th and 5th statements to defend* were formulated:

InGaAs bow-tie diodes are suitable for room temperature active spectroscopic imaging in terahertz frequency range under the conditions of emitters operating in milliwatts power range. Upper limit of imaging frequency range is determined by electron momentum relaxation time. Frequency range for spectroscopic imaging can be extended using plasmonic mixing in nanometer field effect transistors.

Non-coherent room temperature detectors are suitable for spectroscopic imaging systems with optoelectronic terahertz radiation emitters if their noise equivalent power is in order of $10\,\mathrm{pW}/\sqrt{\mathrm{Hz}}$.

5 Conclusions and main results

1. Delta-doped *p-i-n-i* GaAs/AlGaAs heterostructure designed was experimentally investigated under excitation by femtosecond laser pulses. Such structures are effective THz radiation emitters with emitted power exceeding power emitted by InGaAs and InAs surface emitters if optical pump fluence does not exceed $0.7\,\mu J/cm^2$ and $7\,\mu J/cm^2$ for pump pulse repetition rate of 82 MHz ir 1 kHz, respectively.
2. From z-scan experiments optimal excitation conditions were found to achieve efficient THz emission from *p-i-n-i* GaAs/AlGaAs heterostructure. Results were compared with InGaAs and InAs surface emitters.
3. Radiation power of delta-doped *p-i-n-i* GaAs/AlGaAs heterostructure can be enhanced with increasing carrier recombination rate.
4. Using the same theoretical principles as for injection controlled sub-critical Gunn amplifiers, analytical model was created for superlattice diode. It allowed to determine conditions required to create homogeneous electric field. It was showed that if injection diode has a blocking contact homogeneity of electric field can achieved in wide voltage range, meaning that Kroemer point for sub-critical Gunn amplifiers extends to Kroemer interval, i.e. creating thus interval of uniform electric fields.
5. GaAs/AlGaAs superlattice with asymmetric injecting/blocking contacts was investigated experimentally. It was showed that such structure can be used to create homogeneous electric field under range of bias voltage applied.
6. In the injection controlled GaAs/AlGaAs superlattice diode under circumstances of homogeneous electric field created by forward and reversed biased nanosecond DC voltage pulses stable and modulated Bloch gain can be observed in room temperature.
7. The use of focusing optics with short focal distance in the imaging system with a radiation source emitting TEM_{01} beam mode terahertz radiation allows one to record high quality terahertz images with spatial resolution close to diffraction limit.
8. TEM_{01} laser mode was applied for the imaging of silicon solar cells. Selecting appropriate focusing optics results in high quality THz imaging using multimode laser operation.
9. InGaAs bow-tie diodes were applied for room temperature spectroscopic imaging using THz sources with power of the order of milliwatts. High frequency limit is determined by electron momentum relaxation time.

10. Using spectroscopic imaging together with principal component analysis allows one to depict material distribution in THz radiation transparent objects. Such technique was carried out for sucrose and tartaric acid mixed in PTFE matrix.
11. THz frequency range for spectroscopic imaging compared to InGaAs bow-tie diodes can be extended using plasmonic mixing in nanometer field effect transistors coupled with patch type antennas manufactured by 90 nm CMOS technology.
12. Non-coherent room temperature detectors based on titanium microbolometers are suitable for the detection of THz emission and spectroscopic imaging using optoelectronic THz emitters if its noise equivalent power is in the order of 10 pW/$\sqrt{\text{Hz}}$.

References

[1] M. Tonouchi, Cutting-edge terahertz technology, Nature photonics **1**(2), 97–105 (2007).

[2] Q. Lu, N. Bandyopadhyay, S. Slivken, Y. Bai, M. Razeghi, Room temperature single-mode terahertz sources based on intracavity difference-frequency generation in quantum cascade lasers, Applied Physics Letters **99**(13), 131106 (2011).

[3] L. Esaki, R. Tsu, Superlattice and Negative Differential Conductivity in Semiconductors, IBM Journal of Research and Development **14**(1), 61–65 (1970).

[4] A. Reklaitis, Coherence of terahertz emission from photoexcited electron-hole plasma: Hydrodynamic model and Monte Carlo simulations, Phys. Rev. B **77**(15), 153309 (2008).

[5] X. C. Zhang, B. B. Hu, J. T. Darrow, D. H. Auston, Generation of femtosecond electromagnetic pulses from semiconductor surfaces, Applied Physics Letters **56**(11), 1011–1013 (1990).

[6] V. L. Malevich, R. Adomavičius, A. Krotkus, THz emission from semiconductor surfaces, Comptes Rendus Physique **9**(2), 130–141 (2008).

[7] T. Löffler, M. Kreß, M. Thomson, T. Hahn, N. Hasegawa, H. G. Roskos, Comparative performance of terahertz emitters in amplifier-laser-based systems, Semiconductor Science and Technology **20**(7), S134–S141 (2005).

[8] J. Feldmann, K. Leo, J. Shah, D. A. B. Miller, J. E. Cunningham, T. Meier, G. von Plessen, A. Schulze, P. Thomas, S. Schmitt-Rink, Optical investigation of Bloch oscillations in a semiconductor superlattice, Physical Review B **46**(11), 7252–7255 (1992).

[9] J. Faist, F. Capasso, D. L. Sivco, C. Sirtori, A. L. Hutchinson, A. Y. Cho, Quantum cascade laser, Science **264**(5158), 553–556 (1994).

[10] A. Wacker, Lasers: Coexistence of gain and absorption, Nature Physics **3**(5), 298–299 (2007).

[11] P. G. Savvidis, B. Kolasa, G. Lee, S. J. Allen, Resonant crossover of terahertz loss to the gain of a Bloch oscillating InAs/AlSb superlattice., Physical review letters **92**(19), 196802 (2004).

[12] A. Lisauskas, C. Blöser, R. Sachs, H. G. Roskos, A. Juozapavičius, G. Valušis, K. Köhler, Time-resolved photocurrent spectroscopy of the evolution of the electric field in optically excited superlattices and the prospects for Bloch gain, Applied Physics Letters **86**(10), 102103 (2005).

[13] H. Kroemer, Theory of the Gunn effect, Proc. IEEE **52**, 1736 (1964).

[14] D. Dascălu, Small-signal theory of unipolar injection currents in solids, IEEE Transactions on Electron Devices **19**(12), 1239–1251 (1972).

[15] H. Kroemer, The Gunn effect under imperfect cathode boundary conditions, IEEE Transactions on Electron Devices **15**(11), 819–837 (1968).

[16] T. Hyart, N. V. Alexeeva, J. Mattas, K. N. Alekseev, Terahertz Bloch oscillator with a modulated bias., Physical review letters **102**(14), 140405 (2009).

[17] A. J. L. Adam, I. Kašalynas, J. N. Hovenier, T. O. Klaassen, J. R. Gao, E. E. Orlova, B. S. Williams, S. Kumar, Q. Hu, J. L. Reno, Beam patterns of terahertz quantum cascade lasers with subwavelength cavity dimensions, Applied Physics Letters **88**(15), 151105 (2006).

[18] A. Vorobyev, C. Guo, Direct creation of black silicon using femtosecond laser pulses, Applied Surface Science **257**(16), 7291–7294 (2011).

[19] W. Steen, K. G. Watkins, J. Mazumder, *Laser material processing* (Springer Science & Business Media, 2010).

[20] P. Jepsen, D. Cooke, M. Koch, Terahertz spectroscopy and imaging - Modern techniques and applications [Laser Photon. Rev. 5, No. 124-166 (2011)], Laser & Photonics Reviews **6**(3), 418–418 (2012).

[21] X.-C. Zhang, J. Xu, *Introduction to THz wave photonics* (Springer, 2010).

[22] Y. Watanabe, K. Kawase, T. Ikari, H. Ito, Y. Ishikawa, H. Minamide, Component spatial pattern analysis of chemicals using terahertz spectroscopic imaging, Applied Physics Letters **83**(4), 800 (2003).

[23] T. Trzcinski, N. Palka, M. Szustakowski, THz spectroscopy of explosive-related simulants and oxidizers, Bulletin of the Polish Academy of Sciences: Technical Sciences **59**(4), 445–447 (2012).

[24] D. Seliuta, E. Širmulis, V. Tamošiūnas, S. Balakauskas, S. Ašmontas, A. Sužiedėlis, J. Gradauskas, G. Valušis, A. Lisauskas, H. Roskos, K. Köhler, Detection of terahertz/sub-terahertz radiation by asymmetrically-shaped 2DEG layers, Electronics Letters **40**(10), 631 (2004).

[25] A. Juozapavičius, L. Ardaravičius, A. Sužiedelis, A. Kozič, J. Gradauskas, J. Kundrotas, D. Seliuta, E. Širmulis, S. Ašmontas, G. Valušis, H. G. Roskos, K. Köhler, Microwave sensor based on modulation-doped GaAs/AlGaAs structure, Semiconductor Science and Technology **19**(4), S436–S439 (2004).

[26] D. Seliuta, I. Kašalynas, V. Tamošiūnas, S. Balakauskas, Z. Martūnas, S. Ašmontas, G. Valušis, A. Lisauskas, H. Roskos, K. Köhler, Silicon lens-coupled bow-tie InGaAs-based broadband terahertz sensor operating at room temperature, Electronics Letters **42**(14), 825 (2006).

[27] I. Kašalynas, D. Seliuta, R. Simniškis, V. Tamošiūnas, K. Köhler, G. Valušis, Terahertz imaging with bow-tie InGaAs-based diode with broken symmetry, Electronics Letters **45**(16), 833 (2009).

[28] A. Suziedelis, J. Gradauskas, S. Asmontas, G. Valusis, H. Roskos, Giga-and terahertz frequency band detector based on an asymmetrically necked n-n+-gaas planar structure, Journal of applied physics **93**(5), 3034–3038 (2003).

[29] A. Lisauskas, M. Bauer, S. Boppel, M. Mundt, B. Khamaisi, E. Socher, R. Venckevičius, L. Minkevičius, I. Kašalynas, D. Seliuta, G. Valušis, V. Krozer, H. G. Roskos, Exploration of Terahertz Imaging with Silicon MOSFETs, Journal of Infrared, Millimeter, and Terahertz Waves **35**(1), 63–80 (2014).

[30] A. Krotkus, Semiconductors for terahertz photonics applications, Journal of Physics D: Applied Physics **43**(27), 273001 (2010).

[31] J. Trontelj, A. Sešek, Micro-machined millimeter wave sensor array for fm radar application, in *SPIE Security+ Defence* (International Society for Optics and Photonics, 2012), 85440G–85440G.

List of publications related to this thesis

Papers

A1 M. Bauer, R. Venckevičius, I. Kašalynas, S. Boppel, M. Mundt, L. Minkevičius, A. Lisauskas, G. Valušis, V. Krozer, H. Roskos, Antenna-coupled field-effect transistors for multi-spectral terahertz imaging up to 4.25 thz, Optics express **22**(16), 19235–19241 (2014).

A2 I. Kašalynas, R. Venckevičius, G. Valušis, Continuous wave spectroscopic terahertz imaging with ingaas bow-tie diodes at room temperature, Sensors Journal, IEEE **13**(1), 50–54 (2013).

A3 I. Kašalynas, R. Venckevičius, L. Tumonis, B. Voisiat, D. Seliuta, G. Valušis, G. Račiukaitis, Reflective terahertz imaging with the tem01 mode laser beam, Appl. Opt. **52**(23), 5640–5644 (2013).

A4 I. Kašalynas, R. Venckevičius, D. Seliuta, I. Grigelionis, G. Valušis, Ingaas-based bow-tie diode for spectroscopic terahertz imaging, Journal of Applied Physics **110**(11), 114505 (2011).

A5 A. Lisauskas, A. Reklaitis, R. Venckevicius, I. Kasalynas, G. Valusis, G. Grigaliūnaite Vonseviciene, H. Maestre, J. Schmidt, V. Blank, M. Thomson, et al., Experimental demonstration of efficient pulsed terahertz emission from a stacked gaas/algaas pini heterostructure, Applied Physics Letters **98**(9), 091103 (2011).

A6 L. Subačius, R. Venckevičius, I. Kašalynas, D. Seliuta, G. Valušis, J. Schmidt, A. Lisauskas, H. Roskos, K. Alekseev, K. Köhler, Strong electric field driven carrier transport non-linearities in n-type GaAs/AlGaAs superlattices, Acta Physica Polonica A **119**(2), 167–169 (2011).

Patents and other publications

B1 R. Venckevičius, I Kašalynas, G. Valušis, Bow-tie diodes for terahertz imaging: Comparative study, Photonics Letters of Poland **4**(3), pp–103 (2012).

B2 I. Kašalynas, R. Venckevičius, R. Adomavičius, G. Valušis, A. Krotkus, Terahercinių dažnių juostos vaizdinimo sistema, Lietuvos patentas Nr. 6219, paraiškos padavimo data 2013-11-15, patento paskelbimo data 2015-09-25.

B3 R. Venckevičius, I. Kašalynas, G. Valušis, Color photography at terahertz frequencies, SPIE Newsroom, 2016.

Conferences contribution

C1 G. Valušis, L. Minkevičius, V. Tamošiūnas, I. Kašalynas, R. Venckevičius, K. Madeikis, B. Voisiat, D. Seliuta and G. Račiukaitis, Compact optics and detectors for room temperature terahertz imaging systems, 51th International Conference on Microelectronics, Devices and Materials and The Workshop on Terahertz and Microwave Systems, Bled, Slovenia, 2015.

C2 G. Valušis, I. Kašalynas, D. Seliuta, R. Venckevičius, L. Minkevičius, V. Tamošiūnas, B. Voisiat and G. Račiukaitis, Compact Spectroscopic Terahertz Imaging Systems: Sensors and Optics Design, Extended abstracts of 3th international

symposium on Microwave/THz science and applications and 6th International Symposium on Terahertz Nanoscience, Okinawa, Japan, 2015.

C3 I. Kašalynas, R. Venckevičius, R. Adomavičius, G. Valušis, A. Krotkus, A. Švigelj, A. Sešek, L. Pavlovic, J. Trontelj, M. Vinciūnas, Antenna-coupled microbolometer-based THz detectors for room temperature beam profile imaging of the photoconductive THz pulse emitters, 39th international conference on infrared, millimeter, and terahertz waves, Tuscon, AZ, 2014.

C4 J. Trontelj, G. Valušis, R. Venckevičius, I. Kašalynas, A. Sešek, A. Švigelj, A high performance room temperature THz sensor, Terahertz Emitters, Receivers, and Applications IV, San Diego, United States; Proc. SPIE 91990K, 2014.

C5 I. Kašalynas, L. Minkevičius, R. Venckevičius, D. Seliuta, G. Valušis, Multispectral THz imaging with antenna-coupled microbolometers, transistors, and bow-tied diodes, 2nd annual conference of COST action MP1204 and international conference on semiconductor Mid-IR materials and optics : Marburg, Germany, 2014.

C6 I. Kašalynas, A. Švigelj, R. Venckevičius, R. Adomavičius, A. Sešek, L. Pavlovic, G. Valušis, J. Trontelj, Antenna-coupled micro-bolometers for sensitive real-time THz measurements at room temperature, 20 years of quantum cascade laser anniversary workshop : Zurich, Switzerland, 2014.

C7 I. Kašalynas, L. Minkevičius, R. Venckevičius, D. Seliuta, G. Valušis, Multispectral terahertz imaging using compact room temperature operating sensors, GDR-I and GDR workshop on "Semiconductor sources and detectors of THz radiation" : Montpellier, France, 2013.

C8 I. Kašalynas, R. Venckevičius, L. Minkevičius, G. Valušis, Multispectral terahertz imaging with the compact THz detectors designed for room temperature operation / International conference on THz and mid infrared radiation and applications to cancer detection using laser imaging : workgroup meetings of COST actions MP1204 and BM1205 : Sheffield, United Kingdom, 2013.

C9 I. Kašalynas, R. Venckevičius, D. Seliuta and G. Valušis, Imaging and Spectroscopy of Explosives in THz Range, NATO Science and Technology Board Symposium “Innovation for C-IED” (Counter-Improvised Explosive Devices), Military Academy, Vilnius, Lithuania, 2013.

C10 I. Kašalynas, R. Venckevičius, D. Seliuta, L. Tumonis, and G. Valušis, Spectroscopic terahertz imaging with a compact room temperature THz detectors, Proceedings International THz conference 2013, Villach, Austria, 2013.

C11 S. Boppel, A. Lisauskas, M. Bauer, M. Mundt, R. Venckevičius, L. Minkevičius, I. Kašalynas, D. Seliuta, B. Khamaisi, E. Socher, G. Valušis, V. Krozer, H.G. Roskos, Optimized Tera-FET Detector Performance Based On an Analytical Device Model Verified Up To 9 THz, (invited), Programme and Proceedings of the 38th International Conference on Infrared, Millimeter and Terahertz Waves, Mainz on the Rhine, Germany, 2013.

C12 B. Voisiat, L. Tumonis, D. Seliuta, G. Valušis, G. Račiukaitis, I. Kašalynas, R. Venckevičius, High Resolution Reflective Terahertz Imaging With the TEM01 Mode Laser Beam and Large Area Detector, Programme and Proceedings of the 38th International Conference on Infrared, Millimeter and Terahertz Waves,

Mainz on the Rhine, Germany, 2013.

C13 L. Minkevičius, K. Madeikis, I. Kašalynas, R. Venckevičius, D. Seliuta, V. Tamošiūnas, and G. Valušis, Discrete spectrum terahertz imaging using bow-tie diodes: optimized antenna designs and arrays, Terahertz Emitters, Receivers, and Applications IV, San Diego, California, United States; SPIE Proc. Vol. 8846, 2013.

C14 R. Venckevičius, L. Tumonis, I. Kašalynas, G. Valušis, Vaistų ir Sprogmenų Simuliatorių Atpažinimas Teraherciniame Dažnių Ruože, 40-oji Lietuvos Nacionalinė Fizikos Konferencija,Vilnius, Lietuva, 2013.

C15 R. Venckevičius, I. Kašalynas, G. Valušis, Greitaveikių BT-diodų pritaikymas vaizdinimui teraherciniame dažnių ruože, FTMC doktorantų konferencija "FizTech 2012", Vilnius, Lietuva, 2012.

C16 L. Minkevičius, R. Suzanovičienė, G. Molis, A. Krotkus, S. Balakauskas, R. Venckevičius, I. Kašalynas, D. Seliuta, G. Valušis and V. Tamošiūnas, Solar cell imaging and characterization by terahertz techniques, SPIE 2012 Optics+Photonics, San Diego, California, USA, rugpjūčio 12-16, 2012.

C17 L. Minkevičius, R. Suzanovičiene, G. Molis, A. Krotkus, S. Balakauskas, R. Venckevičius, I. Kašalynas, I. Šimkiene, G. Valušis, and V. Tamošiūnas, Terahertz Techniques for Solar Cell Imaging, 31st International Conference on the Physics of Semiconductors, Zurich, Switzerland, 2012.

C18 G. Valušis, L. Minkevičius, I. Kašalynas, R. Venckevičius, D. Seliuta, V. Tamošiūnas, A. Lisauskas, S. Boppel, H.G. Roskos, K. Köhler, Heterodyne and spectroscopic room temperature terahertz imaging using InGaAs bow-tie diodes, 2012 19th International Conference on Microwave Radar and Wireless Communications, Warsaw, Poland, 2012.

C19 L. Tumonis, R. Venckevičius, Terahertz imaging in the reflection Geometry, Open readings, Vilnius, Lietuva, 2012.

C20 I. Kašalynas, R. Venckevičius, D. Seliuta, G. Valušis, Spectroscopic terahertz imaging with the InGaAs-based bow-tie diode, 36th International Conference on Infrared, Millimeter, and Terahertz Waves, Houston, Texas, USA, 2011.

C21 R. Venckevičius, I. Kašalynas, Terahertz imaging of the objects containing sucrose and tartaric acid, Open readings 2011 : 54th scientific conference for young students of physics and natural sciences : Vilnius, Lithuania, 2011.

C22 R. Venckevičius, I. Kašalynas, Furje spektroskopija ir vaizdų užrašymas teraherciniame dažnių ruože, Studentų moksliniai darbai, Vilnius, Lietuva, 2011.

C23 L. Subačius, R. Venckevičius, I. Kašalynas, D. Seliuta, G. Valušis, J. Schmidt, A. Lisauskas, H.G. Roskos, K. Alekseev, K. Köhler, Strong electric field driven carrier transport non-linearities in n-type GaAs/AlGaAs superlattices, 14th International symposium on ultrafast phenomena in semiconductors : Vilnius, Lietuva 2010.

C24 G. Valušis, R. Venckevičius, I. Kašalynas, A. Reklaitis, H. Maestre, J. Schmidt, A. Lisauskas, H.G. Roskos, Efficient $Al_xGa_{1-x}As$ /$Al_{0.45}Ga_{0.55}As$/GaAs heterostructure-based emitter for pulsed terahertz radiation, NATO SET-159 Specialists Meeting on Terahertz and Other Electromagnetic Wave Techniques for Defence and Security, Vilnius, Lithuania, 2010.

Santrauka

Šis darbas skirtas naujų sprendimų paieškai kompaktiškoms terahercinių dažnių ruožo vaizdinimo sistemoms. Jis apima visus jos komponentus - emiterius ir stiprintuvus, modų kokybės problemą bei kompaktiškų kambario temperatūros jutiklių spektroskopiniam vaizdinimui tyrimus.

Šaltinių problematikoje buvo pirmą kartą eksperimentiškai ištirtas heterosandūrinis delta-profiliu legiruotas *p-i-n-i* GaAs/AlGaAs THz emiteris žadinant jį femtosekundinės trukmės optiniais impulsais. Gautus rezultatus palyginus su tokiomis pačiomis sąlygomis žadinamų InGaAs ir InAs paviršinių emiterių duomenimis, nustatyta, kad emiterio galia viršija InGaAs ir InAs paviršinių emiterių emisiją prie tam tikrų sužadinimo sąlygų.

Ieškant naujų THz spinduliuotės stiprinimo aplinkų šiame darbe buvo teoriškai ir eksperimentiškai ištirti diodai su stipriai susietomis GaAs/AlGaAs supergardelėmis. Remiantis kontroliuojamos injekcijos teoriniais principais buvo sukurtas analitinis teorinis modelis diodui su supergardele, reikalingas surasti sąlygas sudaryti vienalytį elektrinį lauką reikalingą Blocho stiprinimui pasireikšti. Eksperimentiškai parodyta, jog kontroliuojamos injekcijos stipriai susietų GaAs/AlGaAs supergardelių diode esant vienalyčiam elektriniam laukui, sukurtam nanosekundinės trukmės nuostovios įtampos impulsais, kambario temperatūroje mikrobangų ruože gali būti stebimas Blocho stiprinimo reiškinys.

Šaltinių modų problematikoje TEM_{01} lazerio moda buvo sėkmingai pritaikyta THz vaizdų užrašymui su didele skiriamąją geba esant 2.52 THz spinduliuotės dažniui. Lazerinis TEM_{01} pluoštas buvo sėkmingai pritaikytas silicio saulės elementų kontaktų kokybės tikrinimui.

Spektroskopiniam THz vaizdinimui buvo pritaikyti inovatyvūs kambario temperatūros kompaktiški terahercinės spinduliuotės detektoriai. Asimetriškai susiaurinti InGaAs detektoriai buvo panaudoti sacharozės ir vyno rūgšties bandinių vaizdinimui ir jų komponentinės sudėties nustatymui dažnių ruože nuo 0.5 iki 2.52 THz. Vaizdinimui naudojama dažnių sritis buvo išplėsta iki 4.25 THz panaudojant, detektorius su antenomis kaupinamais lauko tranzistoriais, veikiančiais plazmoninio maišymo principais. THz vaizdinimo sistemoms su mažos vidutinės galios optoelektroniais emiteriais buvo pritaikyti antena kaupinami titano mikrobolometrai. Nustatyta, kad jų maža 10 $\mathrm{pW}/\sqrt{\mathrm{Hz}}$ eilės triukšmų ekvivalentinė galia leidžia juos panaudoti optoelektroninių emiterių THz spinduliuotės detekcijai bei objektų spektroskopiniam vaizdinimui THz dažnių ruože.

Information about the author

Name surname	**Rimvydas Venckevičius**
Birth date and place	July 8, 1986, Šilutė, Lithuania
E-mail	rimvydas.venckevicius@ftmc.lt

Education

2005 m.	Secondary education in Šilutės pirmoji Gymnasium
2009 m.	Bachelor degree in Applied Physics, Faculty of Physics of Vilnius University
2011 m.	Master degree (Magna um laude diploma) in Material Science and Semiconductor Physics, Faculty of Physics of Vilnius University
2011–2016 m.	Doctoral studies in Center for Physical Science and Technology

Scientific experience

Since 2008	Engineer, junior-researcher in Center for Physical Sciences
Since 2010	Participation in 3 projects supported by Reasearch Council of Lithuania; 1 project supported by Agency for Science, Innovation and Technology of Lithuania; 1 project supported by European Social Fund Agency; 1 project supported by European Defence Agency Programme.

Internship

2009/07/09–2009/09/30	Erasmus training in Physikalisches Institut, Johann Wolfgang Goethe Universität, Frankfurt/M, Germany

Specialization	Investigation of emitters, detectors and optical components in terahertz frequency range, spectroscopic terahertz imaging techniques, Fourier transform spectroscopy, transmission line technique with nanosecond DC voltage pulses, Microwave technique, programming in LabVIEW environment